PHILOSOPHICAL TRANSACTIONS OF THE ROYAL SOCIETY A MATHEMATICAL, PHYSICAL & ENGINEERING SCIENCES

Controls on the physics and chemistry of seafloor hydrothermal circulation

Adam Schultz and Henry Elderfield

Phil. Trans. R. Soc. Lond. A 1997 **355**, 387-425
doi: 10.1098/rsta.1997.0014

Controls on the physics and chemistry of seafloor hydrothermal circulation

By Adam Schultz and Henry Elderfield

University of Cambridge, Department of Earth Sciences, Downing Street, Cambridge CB2 3EQ, UK

Low temperature diffuse hydrothermal circulation is a natural consequence of the cooling of the oceanic lithosphere. Diffuse flow is expected to be ubiquitous, and will be present both within mid-ocean ridge crest axial zones of young age (0–1 Ma), and also on the older ridge crest flanks and limbs. If underlying thermal models are correct, hydrothermal circulation should persist for oceanic lithosphere of age 0–65 Ma, and is present over half the total area of the ocean basins. By using numerical models of hydrothermal circulation in cracked permeable media, we show qualitatively how diffuse flow is an intrinsic feature of high temperature axial (0–1 Ma) hydrothermal systems, and is not restricted to older (more than 1 Ma) lithosphere. This is in agreement with our field observations which suggest that in such high temperature vent fields the greatest part of the heat and volume flux is due to lower temperature diffuse flow, rather than high temperature black smoker venting.

By combining direct measurements of the physical properties of diffusely flowing effluent within axial hydrothermal systems with concurrent sampling of the chemical properties of that effluent, and by considering also the chemistry of unmixed black smoker endmember fluids from the same hydrothermal systems, the processes of mineral deposition and dissolution can be studied directly. By referring to the present-day lithology of such areas, it is possible to examine the balance between concurrent mineral deposition and dissolution processes, and the retention rate of specific mineral assemblages integrated over the history of the hydrothermal system. Thus details of the episodicity of hydrothermal venting within the system may be revealed. An example of this method of combining a variety of direct measurements of diffuse and high temperature effluent properties is given from the TAG hydrothermal field, Mid-Atlantic Ridge.

Long time series observations of the physical properties of diffuse and high temperature effluent reveal the importance both of tidal variability and also the response to changes in the permeability structure of the system brought about by natural and anthropogenic processes. Several mechanisms are considered to explain the relationship between ocean tidal loading, solid Earth tidal deformations, and the observed changes in flow within axial hydrothermal systems.

1. Introduction

The dominant means by which the newly emplaced axial (age 0–1 Ma) oceanic lithosphere is cooled is through the advection of seawater into, and circulation through, the cracked permeable seafloor. The higher temperature part of that process has

Phil. Trans. R. Soc. Lond. A (1997) **355**, 387–425
Printed in Great Britain

received the greatest theoretical and experimental interest since the initial discovery of high temperature venting in the Galapagos (Corliss *et al.* 1977). In the present paper we consider the lower temperature more diffuse component of that circulation. Diffuse hydrothermal fluids circulating through the oceanic lithosphere and subsequently emitted into the water column present an observational challenge. This mode of flow is associated with low rates of fluid transport. Diffuse effluent temperature may be elevated only slightly above that of ambient seawater, and diffuse effluent velocity may span the range of centimetres per second (Schultz *et al.* 1992) down to rates just in excess of molecular diffusion. Furthermore, plumes of hydrothermal effluent resulting from diffuse sources may not necessarily be entrained into local high temperature plumes, and thus might not be carried into the water column efficiently (Schultz *et al.* 1992; Rosenberg *et al.* 1988).

Under certain conditions diffuse plumes may be sufficiently saline when mixed with seawater such that they are non-buoyant (Turner & Gustafson 1978), and thus may have little signature in the overlying water column. It is possible that effluent may pool along the seafloor, or under the appropriate range of physical and chemical conditions, may form warm briny submarine aquifers. This complicates efforts to quantify hydrothermal fluxes within such systems.

It is therefore appropriate to consider further the physics and chemistry of the lower temperature component of seafloor hydrothermal circulation, and to give special attention to the observational problems these fluids entail. Constraints on the total heat flux available to drive hydrothermal circulation globally and the distribution of that flux with lithospheric age are based largely on parametric thermal models. We review in some detail the assumptions behind these underlying models and discuss the uncertainties that arise in estimates of the total volume of seawater circulating through and interacting with the oceanic lithosphere.

We present data obtained from direct seafloor measurements of the physical and chemical properties of diffuse hydrothermal effluent. These were obtained during the joint British–Russian BRAVEX/94 MIR submersible expedition to the TAG (26°08′ N, 44°49′ W) and Broken Spur (29°10′ N, 43°10′ W) vent fields, Mid–Atlantic Ridge, during the period August–October 1994. Further data were recovered during the joint US-British Atlantic II Alvin Leg 132–02 return expedition to TAG in February–March 1995. The samples were obtained from the 'Medusa' hydrothermal monitoring system, a set of instruments that capture fluid samples and measure effluent velocity and temperature directly at the point of emission on the seafloor (Schultz *et al.* 1996). These instruments were used to monitor the hydrology of the TAG mound before, during and after Ocean Drilling Program (ODP) leg 158, and also to map the advective component of heat flux density during those times.

2. Underlying thermal models

It is the cooling of the newly formed oceanic lithosphere that provides the source of heat to drive hydrothermal circulation. In the following section we review the underlying theoretical and observational basis of our understanding of that process.

We consider two methods of establishing the total budget of heat available to drive global seafloor hydrothermal circulation. The first method is based on considering the thermal behaviour of the oceanic lithosphere as equivalent to that of a conductively cooled plate. The second method considers the total global ridge crest magmatic

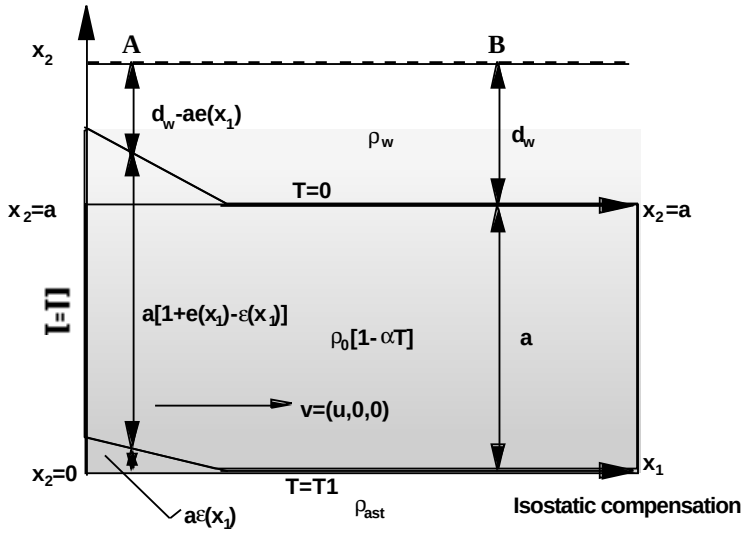

Figure 1. Schematic diagram of lithospheric cooling represented by conduction through a two-dimensional plate heated from the side and below.

budget and uses this, as well as knowledge of the latent heat of crystallization and the specific heat of seawater to place bounds on the heat available to drive hydrothermal circulation.

(*a*) *Conductively cooled plate model*

The difference between the heat flow predicted from a model representing the purely conductive cooling of the oceanic lithosphere (McKenzie 1967) and that observed globally from seafloor heat flow measurements is taken to be due to the heat carried away from the slab through advection, i.e. seafloor hydrothermal circulation and venting. This follows a tradition dating back at least as far as Parsons & Sclater (1977).

In the Parsons & Sclater model (figure 1), T is temperature, T_1 is a constant temperature applied to the base of the model and to the vertical planar origin at horizontal distance $x_1 = 0$, α is the thermal expansion coefficient, ρ_{w} the density of seawater, ρ_0 the density of 0 °C lithosphere, ρ_{ast} the density of aesthenosphere, d_{w} the asymptotic depth to the seafloor at large distances from the ridge, a the asymptotic thickness of the lithosphere, and $a\epsilon(x_1)$ is the displacement of the bottom of the lithosphere above a somewhat arbitrary level of compensation. The ridge is elevated above such a reference level due to the thermal expansion of the hotter materials near the ridge crest relative to the thermal contraction of cooler materials at distance from the ridge.

The topographic anomaly due to thermal expansion effects is (Davis & Lister 1974)

$$h = \alpha_{\mathrm{eff}} \int_0^\infty \{T_1 - T(z)\}\,\mathrm{d}z = (2/\sqrt{\pi})\alpha_{\mathrm{eff}} T_1 \sqrt{\kappa t}, \tag{2.1}$$

where α_{eff}, the effective thermal expansion coefficient, is modified for isostatic equilibrium (i.e. the material expands thermally but then is further compressed or dilated through changes in hydrostatic pressure due to changes in the height of the overlying

water column) thus

$$\alpha_{\text{eff}} = \frac{\rho_0}{\rho_0 - \rho_{\text{w}}}\alpha. \tag{2.2}$$

The assumption of isostatic equilibrium is justified on the basis of marine gravity data. These reveal that on a gross scale mid-ocean ridges are not associated with significant free-air gravity anomalies. By assuming perfect isostasy we take the lithosphere to float atop a semi-fluid aesthenosphere, which is equivalent to maintaining a constant-pressure zone at depth. There is therefore no mechanical impediment to the subsidence of oceanic lithosphere after cooling.

The non-dimensional heat transport equation is given for the present example by Parsons & Sclater (1977),

$$\frac{\partial^2}{\partial x_1'^2}T' - 2Pe\frac{\partial}{\partial x_1'}T' + \frac{\partial^2}{\partial x_2'^2}T' = 0, \tag{2.3}$$

where the primes denote non-dimensional variables $T = T_1T'$, $x_1 = ax_1'$, and $x_2 = ax_2'$. The Peclet number (i.e. the thermal Reynolds number, e.g. the ratio of heat convection to heat conduction) is given by $Pe = ua/2\kappa$, where κ is the thermal diffusivity and u is the ridge crest half-spreading rate.

The solution for the non-dimensional heat flow equation which satisfies the boundary conditions given in figure 1 is

$$T = (1 - x_2) + 2\sum_{n=1}^{\infty}\frac{(-1)^{n+1}}{n\pi}\sin(n\pi x_2)\mathrm{e}^{-\mu_n x_1}, \tag{2.4}$$

where

$$\mu_n = [(Pe^2 + n^2\pi^2)^{1/2} - Pe]. \tag{2.5}$$

When the product of the age of the lithosphere and the thermal diffusivity is much less than the square of the asymptotic plate thickness, the above relationship assumes the form

$$T \sim \mathrm{erf}[1 - x_2'/2t^{1/2}]. \tag{2.6}$$

Lister (1972) obtained the above expression for the temperature inside a semi-infinite halfspace cooled from a uniform temperature through vertical conduction. Parsons & Sclater (1977) find that the general solution to the two-dimensional heat flow equation reduces to Lister's halfspace form also when $x_1'Pe \gg 2$. For a reasonable set of thermal conductivities this condition holds for all lithosphere older than 1 Ma regardless of the spreading rate.

(i) *Predictions of bathymetry and heat flow*

From the Parsons & Sclater model one can predict simultaneously the bathymetric height and the heat flow due to thermal conduction for seafloor of a given age. There is good agreement, to first order, between observed broad-scale seafloor bathymetry and that predicted from the cooling plate model (Parsons & Sclater 1977; Sclater *et al.* 1980; Stein & Stein 1992, 1994), i.e. the height of the seafloor scales proportionally with the square-root of age. While Carlson & Johnson (1994) suggest that the cooling plate model fails to fit seafloor bathymetry systematically for lithospheric ages greater than 81 Ma, this is a second order effect, and is observed for ages at which there is no longer direct evidence of hydrothermal circulation.

The general concurrence between the predicted and observed seafloor bathymetry

suggests strongly that the underlying thermal model approximates to a reasonably accurate degree the product of the true temperature distribution and the effective coefficient of thermal expansion. This is in dramatic contrast to predictions of heat flow (rather than bathymetry) from the cooling plate model which overestimate the true heat flow for lithospheric ages less than approximately 50 Ma. Furthermore, the Parsons & Sclater model underestimates the true heat flow and overestimates the true seafloor bathymetric depths for ages greater than 70 Ma.

(ii) *Vertical extent of hydrothermal circulation*

There is considerable evidence that the 'reaction zone', i.e. the region at which there is direct interaction between newly injected magma and hydrothermal fluids is found at 2.5 km (±2.0 km) depth throughout much of the global ridge crest system. Seismic data from a variety of ridge crest segments show the presence of a low velocity layer consistent with the existence of magma chambers. Two-way travel time data for a multichannel wide aperature profile obtained from 9°30′–10° N on the East Pacific Rise (Vera & Diebold 1994) show a low velocity zone at depths varying between 1390–1600 mbsf along the strike of the ridge axis. Other studies reveal similar structures at depths spanning 2300–2400 mbsf beneath the Juan de Fuca Ridge (Morton 1984), 3500 mbsf beneath the Lau Basin (Morton & Sleep 1985), and elsewhere.

Silica geobarometry reinforces further the extent of the depth of high temperature water–rock interactions. Von Damm *et al.* (1985) note that dissolved SiO_2 concentration is often in equilibrium with solid quartz. Quartz solubility is a function of both temperature and pressure. If the silica content of the hydrothermal effluent is measured, and the temperature can be determined separately, then the remaining unknown – pressure – can also be determined. Curves of silica dissolution *vs* temperature for various pressures are given, e.g. in Kennedy (1950) and in various solutions by Chen & Marshall (1982).

The temperature of black and white smoker vent fluids is measured routinely at the base of smoker chimney orifices. The pressure can be assumed to be hydrostatic in a crack-dominated hydrothermal system, and the depth of the water column is known. The pressure calculated from the silica concentration can therefore be transformed to depth within the hydrothermal system, i.e. the depth where the silica dissolution took place. Von Damm *et al.* (1985) report that depths determined in this way span 0.5–3.5 km at sites in their original study. Subsequent work tends to confirm this depth range.

Hydrothermal circulation is therefore likely to be concentrated within the upper 2–3 km of the oceanic lithosphere. As a result, only the uppermost few percent of any vertical lithospheric section will be affected directly by advective heat loss. Hydrothermal circulation will therefore play little role in changing the broad-scale bathymetry of the seafloor. In contrast, the heat flow will be influenced directly by the removal of heat from the upper part of the lithosphere through the advective losses due to hydrothermal discharge.

Before taking the existing framework and using it to place bounds on the global hydrothermal heat flux budget, it is necessary to refine the underlying thermal model. We consider initially the Stein & Stein (1992, 1994) reformulation of the Parsons & Sclater model. This differs from the original in that it is expressed in terms of

bathymetric depth, rather than height above a hard-to-define compensation depth,

$$T(x,z) = T_1\left[\frac{z}{a} + \sum_{n=1}^{\infty} c_n \mathrm{e}^{-\mu_n(x/a)} \sin\left(n\pi\frac{z}{a}\right)\right], \tag{2.7}$$

where $c_n = 2/(n\pi)$ and the other quantities match those in Parsons & Sclater (1977). The equation for surface heat flux density may be written

$$q(x) = k\left(\frac{\partial T}{\partial z}\right)_{s=0} = q_s\left[1 + 2\sum_{n=1}^{\infty} \mathrm{e}^{-\mu_n(x/a)}\right], \tag{2.8}$$

where $q_s = kT_1/a$ is the asymptotic heat flow for old lithosphere in which the thermal gradient is linear (Stein & Stein 1992).

The bathymetric depth to the seafloor vs. distance from the spreading centre is

$$d(x) = d_{\mathrm{w}}\left[2 - \frac{8}{\pi^2}\sum_{n=1,\mathrm{odd}}^{\infty} n^{-2}\mathrm{e}^{-\mu_n(x/a)}\right] - ae(0), \tag{2.9}$$

where $d_{\mathrm{w}} - ae(0)$ is the bathymetric depth to the top of the ridge axis as seen in figure 1, and d_{w} (the depth to the top of the asymptotically old lithosphere) is given by

$$d_{\mathrm{w}} = \frac{\alpha\rho_{\mathrm{ast}}T_1 a}{2(\rho_{\mathrm{ast}} - \rho_{\mathrm{w}})}. \tag{2.10}$$

Stein & Stein (1992, 1994) conducted a model search where the free parameters were the asymptotic thickness of the lithosphere, the base temperature, and the coefficient of thermal expansion. The best fitting coefficient of thermal expansion was found to be $\alpha = 3.1 \times 10^{-5}\ \mathrm{K}^{-1}$, the best fitting plate thickness was 95 km, and the best fitting basal temperature was 1450 °C. The asymptotic depth to the top of the lithosphere in this model is 5651 m, and the asymptotic heat flow is 48 mW m^2.

The Stein & Stein reformulation of the Parsons & Sclater conductively cooled plate model is an improvement over its direct ancestor as it fits gross bathymetry data and heatflow data exceptionally well (except for heat flow for ages less than 50–75 Ma). The RMS misfit between calculated and observed bathymetric depths was 0.42, and for heat flow values, 0.40. Corresponding values for the Parsons & Sclater model were 1.0 and 0.83. From a purely statistical point of view, both models are acceptable, but the reliability of these models is difficult to appraise in the absence of a sensitivity analysis.

An additional caveat is that the cooling plate model is two-dimensional and based on fitting data sets that have been grouped according to age and spreading rate and thus represent global averages. This ignores smaller-scale heterogeneities in heat flow which can accommodate (locally) much larger components of hydrothermal cooling, as well as areas where there may be no appreciable misfit between the conductive cooling model and the local observations and thus no direct surface evidence for hydrothermal circulation.

Stein & Stein find that the conductively cooled plate model fits observed heat flow adequately at ages greater than 65 ± 10 Ma. This is often referred to as the 'sealing age', and has been interpreted in the past to represent a critical age in oceanic lithosphere where significant levels of hydrothermal circulation are no longer supported due to a drop in the permeability of the basement rock. Alternatively, it has been interpreted as the age of lithosphere associated with sufficient sedimentary cover such

that underlying circulation cells are contained entirely within an impermeable cap, and have no surface heat flow expression.

The heat flow deficit at younger ages is attributed to hydrothermal circulation in the oceanic lithosphere. Elder first speculated on this in 1965. This was followed up by LePichon & Langseth (1969). Finally Lister (1972) provided a theoretical basis for predicting that the heat deficit could be explained best by hydrothermal circulation, and it is arguable that it is to Clive Lister we owe the credit for the first prediction of concentrated hydrothermal circulation at ridge crests, i.e. smoker vent fields and the like.

The conductive heat flux density may be represented in this model by

$$\left.\begin{aligned} q'(t) &= 510t^{-1/2}\ \mathrm{MW\ m^{-2}}, \quad t \leqslant 55\ \mathrm{Ma}, \\ q'(t) &= 48 + 96\mathrm{e}^{-0.0278t}\ \mathrm{MW\ m^{-2}}, \quad t > 55\ \mathrm{Ma}. \end{aligned}\right\} \tag{2.11}$$

where t is lithospheric age in Ma. In order to determine the total heat flux for the oceanic lithosphere, i.e. the heat flux density integrated over the upper surface area of the lithosphere, it is necessary to divide the lithosphere into a number of bands of different age, determine the average heat flux density for each of these bands, and their respective surface areas.

The expressions for heat flux density (2.11) take the form of the Lister (1972) halfspace cooling approximation. Stein & Stein report that use of the full series expansion rather than this approximation changes the result by 0.4%, even when a modified side boundary condition due to Davis & Lister (1974) is used which conserves energy by balancing the total heat flux, convective plus conductive, from the origin with that convected at the supply temperature T_1, ignoring the latent heat of the small melt volume (i.e.)

$$-k\frac{\partial T}{\partial x} + \rho c_\mathrm{p} u T = \rho c_\mathrm{p} u T_1, \tag{2.12}$$

or in non-dimensional terms

$$\frac{-1}{2Pe}\frac{\partial}{\partial x'}T' + T' = 1|_{x'=0} \tag{2.13}$$

rather than the original Parsons & Sclater (1977) isothermal boundary condition, i.e. $T = 1$ at $x = 0$. Note here that c_p is the specific heat. This new boundary condition equates the heat introduced at the origin by magma injection to balance that lost to horizontal conduction and to advection by horizontal motion of the plate.

It is intuitively appealing that there should be a heat balance in the steady state, but that imposed balances only horizontal advection/diffusion. An additional term involving advection of heat due to hydrothermal circulation must be considered. Certain aspects of Sleep's (1975) boundary conditions are also appealing, as they attempt to bring in the behaviour of melt including energy in the form of latent heat into the balance, which is ignored here. It is not clear that the approximation that latent heat may be ignored due to small melt volumes is necessarily true, particularly at faster spreading ridges where larger quantities of melt are expected.

Stein & Stein (1994) calculate the integrated heat flux for oceanic lithosphere of ages less than t_n as

$$Q'_n = \sum_{i=1}^{n} A_i q'_i, \tag{2.14}$$

Table 1. *Global heat budget*

(Observed and model conductive heat flows, and residual cumulative heat flow presumed due to hydrothermal advection, adapted from Stein & Stein (1994).)

cumulative ages (Ma)	predicted	observed	hydrothermal
1	3.6	0.4 ± 0.3	3.2 ± 0.3
2	5.1	1.0 ± 0.7	4.1 ± 0.7
4	7.2	1.8 ± 1.4	5.4 ± 1.4
9	11.3	3.8 ± 2.1	7.4 ± 2.1
20	15.6	6.5 ± 2.7	9.1 ± 2.7
35	19.8	9.2 ± 3.2	10.5 ± 3.2
52	22.7	11.5 ± 3.4	11.2 ± 3.4
65	24.6	13.3 ± 3.5	11.3 ± 3.5
80	26.9	15.6 ± 3.7	11.3 ± 3.7
95	28.5	17.3 ± 3.9	11.2 ± 3.9
110	29.8	18.7 ± 3.9	11.1 ± 3.9
125	30.6	19.5 ± 3.9	11.1 ± 3.9
140	31.5	20.4 ± 3.9	11.1 ± 3.9
160	31.9	20.8 ± 3.9	11.1 ± 3.9
180	32.0	21.0 ± 3.9	11.0 ± 3.9

where A_i is the total surface area for lithosphere spanning ages t_{i-1} and t_i, and q'_i is the average heat flux density for lithosphere spanning those ages as predicted by the cooling plate model. Similarly, the observed integrated heat flux is

$$Q_n = \sum_{i=1}^{n} A_i q_i, \tag{2.15}$$

where q_i is the observed average heat flux density for that age range.

The difference between the integrated heat flux for the lithosphere of age less than t_n predicted by the thermal model and the observations is

$$Q_n^h = Q'_n - Q_n = \sum_{i=1}^{n} A_i (q'_i - q_i), \tag{2.16}$$

which is taken to be the total heat flux due to hydrothermal circulation integrated over all oceanic lithosphere younger than t_n.

The results of these calculations are summarized in table 1 which contains the cumulative ages of the seafloor from zero age, the heat flow in TW (1 TW = 10^{12} W) predicted from this model, the heat flow actually observed as a global average for oceanic lithosphere of the specified cumulative age, and the difference which is taken to be the total budget available to drive hydrothermal circulation of cool seawater into the cooling oceanic lithosphere.

Stein & Stein (1994) calculate from their catalogue of heat flow observations that the total ocean lithospheric heat flux is 32 TW. From the misfit to the cooling plate model, they predict that of this total budget, 11 ± 4 TW, or 34 ± 12% is due to hydrothermal circulation processes (this includes ridge crests and ridge flanks out to

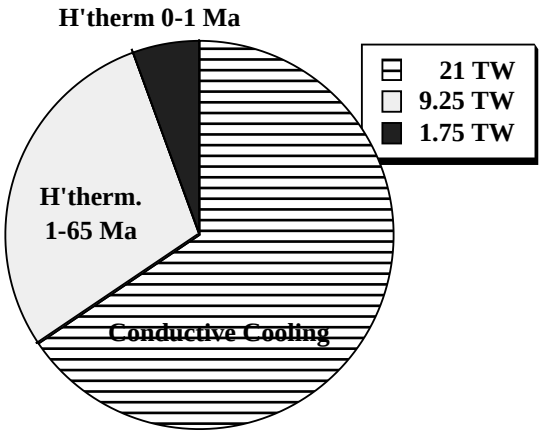

Figure 2. Total heat budget of the oceanic lithosphere showing relative partitioning between heat lost through conductive cooling and heat lost through advection of hydrothermal fluids. The advective component is subdivided into ridge crest axial hydrothermal flow for lithosphere no older than 1 Ma, and the remaining 64 Ma of lithosphere where hydrothermal circulation persists unambiguously.

the 'sealing age' of 65 ± 10 Ma). It is clear that the greatest part of hydrothermal circulation occurs in older crust far from the 'active' circulation found at ridge crests. The division between conductive cooling, off-axis hydrothermal advective cooling, and on-axis hydrothermal cooling is seen in figure 2.

(*b*) *Persistence of hydrothermal circulation in older lithosphere*

There is evidence from K/Ar dating of celadonites (a low-temperature, e.g. less than 30 °C) alteration mineral) in the Troodos ophiolite complex that low-temperature hydrothermal alteration persisted there for at least 40 Ma after crustal formation (Gallahan & Duncan 1994). Localized depressions in predicted heat flow values from areas such as the equatorial Pacific basin are consistent with thermal circulation and large-scale lateral advection of water through basaltic crust. Analysis of major elements in fluids extracted from sediment pores in this region appear to corroborate this view, and to show evidence for hydrothermal circulation for ocean lithospheric ages spanning 15–70 Ma (Baker *et al.* 1991).

Direct evidence of off-axis hydrothermal flow at elevated temperatures has been obtained in recent years on the eastern flank of the Juan de Fuca Ridge (Davis *et al.* 1992; Wheat & Mottl 1994). There is additional evidence for off-axis hydrothermal circulation from a variety of theoretical and observational studies. These include numerical solutions for broad-scale flow within permeable media heated from below (Fehn *et al.* 1983), tank experiments using Hele-Shaw cells (Hartline & Lister 1981), and from observations of the large-scale fabric of the seafloor in the form of ridge-parallel faults (Johnson *et al.* 1993). Persistent zones of in-flow and out-flow, either channelled through permeable pathways following seafloor faults, or as an intrinsic feature of convection in permeable media (or both) are therefore expected over broad areas of the flanks and limbs of the ridge crests and older oceanic lithosphere. The heat flux models described thus far would suggest that the occurrence of off-axis systems of the Juan de Fuca–flank type should not be uncommon.

(i) *Lithospheric cooling models accommodating hydrothermal sinks and magmatic sources*

The cooling plate model does not contain hydrothermal circulation explicitly, thus the hydrothermal component is constrained only weakly. Morton & Sleep (1985) re-examined Sleep's (1975) model of a dyke annealing to the vertical boundary at the origin of a ridge crest spreading centre. A new term is added to the original two-dimensional heat flow equation,

$$u\frac{\partial T_{\mathrm{e}}}{\partial x} = \frac{k}{\rho c_{\mathrm{p}}}\left(\frac{\partial^2 T_{\mathrm{e}}}{\partial x^2} + \frac{\partial^2 T_{\mathrm{e}}}{\partial z^2}\right) + \frac{H}{\rho c_{\mathrm{p}}}, \tag{2.17}$$

where T_{e} is the excess temperature in °C (i.e. the temperature at a given position within the model lithosphere less the steady state solution for the asymptotic temperature at $x = \infty$), z is the depth below the top of the oceanic lithosphere, k is the thermal conductivity, ρc_{p} is the volume specific heat, and H represents all excess sources and sinks of heat including heat brought in by intrusion, latent heat of crystallization, and heat removed by hydrothermal circulation.

The appropriate boundary conditions are:

$$T_{\mathrm{e}} = 0|_{z=0} \qquad \text{(i.e. no excess temperature at the seafloor);}$$

$$T_{\mathrm{e}} = 0|_{z=\lambda} \qquad \text{(i.e. no excess temperature at the base of the lithosphere);}$$

$$T_{\mathrm{e}} = 0|_{x=\infty};$$

$$\frac{\partial T_{\mathrm{e}}}{\partial x} = \left.\frac{u\phi c_{\mathrm{p}} T_{\mathrm{e}}}{k}\right|_{x=0}.$$

where λ is the depth to the base of the lithosphere. The final boundary condition balances advection and diffusion across the point of dyke injection at the origin.

This solution to the heat flow equation does not reduce to the simple form found in Sleep (1975), but it does remain tractable if one assumes a simple form for the heat sources and sinks. Morton & Sleep (1985) take this to be a Dirac delta function located a distance x_0 from the origin (i.e. an infinitesimally thin spike of unit area centred at $x = x_0$). Therefore, hydrothermal circulation is modelled as a set of infinitesimally thin heat sinks. This is inadequate to represent the details of flow, or of any chemical reactions taking place within such a flow regime, but it is adequate to understand the impact of localized hydrothermal convection on the broad-scale heat budget of a cooling plate.

Morton & Sleep (1985) take the top of a magma chamber to represent the 1185 °C isotherm, which they associate with the 70% solid temperature of MORB (Mid-Ocean Ridge Basalt). Morton & Sleep note that in magma chamber models based on ophiolite studies and thermal models, most of the latent heat of crystallization is released at the top of the chamber, resulting in plated gabbros and crystals that settle to form cumulate layers. A small amount of melt may be retained in the crystal mush and may crystallize at the sides of the magma chambers. This is used as justification for placing 70% of the latent heat resulting from magma chamber crystallization along the top of the magma chamber, and the remainder along the sloping sides. Latent heat resulting from crystallization of dykes and flows is placed directly above the chamber, on-axis.

The model is constructed by placing all of the latent heat initially at the ridge axis in order to determine the temperature distribution in the plate (as before). By so

doing, it is possible to identify the 1185 °C isotherm. The latent heat is then redistributed on the top and sides of the magma chamber (i.e. along the 1185 °C isotherm), thereby changing the temperature field and shifting the 1185 °C isotherm. The final model is constructed by carrying out this process iteratively until the isotherms converge to a stable geometry such that the location of the 1185 °C isotherm corresponds to the latent heat distribution.

Morton & Sleep find that the depths to the 1185 °C isotherm tend to be shallower than the depths to the tops of the corresponding axial magma chambers, at least as inferred from seismic observations. This situation is rectified if one introduces a set of heat sinks representing heat loss due to hydrothermal flow. By introducing a (non-unique) set of sinks, the isotherm may be depressed such that its contour matches that of the presumed magma chamber.

In order to quantify the total budget of heat available to drive hydrothermal circulation, we make use of the best features of the Stein & Stein (1992, 1994) model and the Morton & Sleep (1985) boundary conditions. The details of such a model may be found in Stein *et al.* (1995).

The constraints on this model are the depth and heat flow data for older ages (which constrain the overall thermal model), earthquake and magma chamber depths (which constrain the near-axial geotherm), and the heat flow data for 10–50 Ma (which constrain the surface temperature gradient for these ages). Furthermore, two sets of models are produced for two different classes of spreading rates. For lithospheric ages greater than 0.5 Ma, the difference between the two spreading rate models is small, and they may be combined. For ages between 0.5 Ma and 50 Ma, the predicted model heat flow is approximated by $q_c = 308t^{-1/2}$, where q is in mW m^{-2}, and t is in Ma.

The Stein *et al.* composite model predicts a higher heat loss for ages less than 10 Ma than the simple conductively cooled plate model. This adjusts the hydrothermal component of heat loss (i.e. the mismatch between the model prediction and the observations) by lowering slightly the hydrothermal component relative to the simpler model. Regardless of this detail, the majority of cumulative hydrothermal heat loss remains associated with ages greater than 1 Ma. Another result of these calculations is that higher rates of hydrothermal heat loss are associated with faster spreading rates than slow spreading rates.

(ii) *Predicted hydrothermal heat loss per unit length ridge axis*

The Stein *et al.* (1995) model permits us to estimate the predicted heat flux density at each point on the oceanic lithosphere, and to integrate over surface areas of a given age to determine the cumulative hydrothermal heat flux due to crust of a given age range. Stein *et al.* (1995) assume that sediment cover does not control the 'sealing age' but Davis *et al.* (1992) dispute this view, at least on a local scale. Therefore, it should be remembered that if the sediment cover on a ridge is unusually thick for its age, the surface heat expression may be reduced or suppressed.

For slow-spreading plate boundaries (e.g. half rates of 10 mm yr^{-1}), the model predicts the hydrothermal heat flux would be the product of 1 W m^{-2} average heat flux density with the total area on both sides of the ridge axis within 0.1 Ma, or 2 MW km^{-1} of ridge axis for lithosphere younger than 0.1 Ma. For half rates of 30 mm yr^{-1} (e.g. Juan de Fuca Ridge), the equivalent value is 15 MW km^{-1} of ridge axis.

For older ocean lithosphere (older than 0.5 Ma), the slow spreading and fast spread-

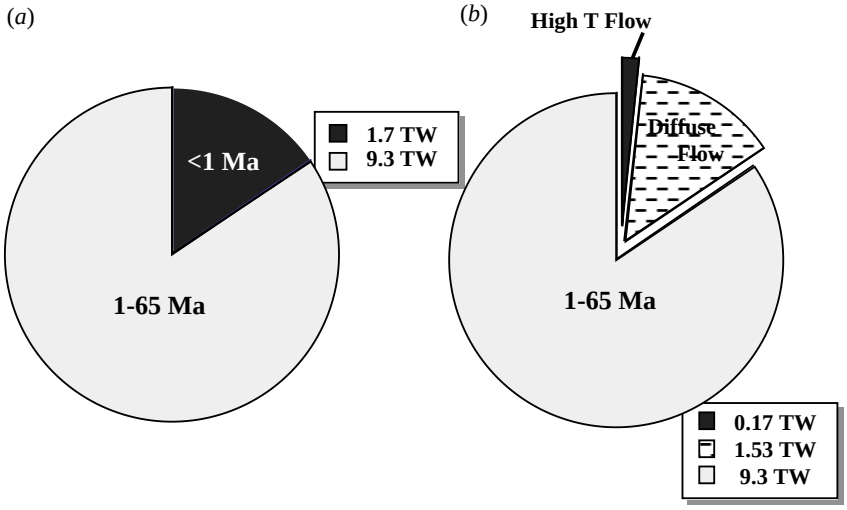

Figure 3. Total hydrothermal heat budget of the oceanic lithosphere (left). The advective component is subdivided into ridge crest axial hydrothermal flow for lithosphere no older than 1 Ma, and the remaining 64 Ma of lithosphere where hydrothermal circulation persists unambiguously (right).

ing models are almost indistinguishable. Stein *et al.* (1995) estimate that the total heat flux density budget for hydrothermal circulation averaged over ages of 0–1 Ma is *ca.* 0.5 W m^{-2} × (3.5 × 10^6 km^2 surface area for crust of that age) (Stein & Stein 1994) yielding a total heat flux of 1.75 TW.

Recall that Stein & Stein (1994) estimated that the total ocean lithospheric heat flux is 32 TW, of which 11 ± 4 TW, or 34 ± 12% is due to hydrothermal circulation processes (including ridge crests and ridge flanks out to the 'sealing age' of 65 ± 10 Ma). While Stein *et al.* (1995) have made no similar calculation of the total budgets integrated over all crustal ages for the improved composite model, the cumulative budgets will be qualitatively the same as the earlier model. If so, then hydrothermal heat flux in the near-axial zone (0–1 Ma) accounts for only *ca.* 16% of the total hydrothermal heat flux budget for ages (0–65 Ma). The partitioning of the total budget of hydrothermal heat flux between on-axis (0–1 Ma) and off-axis (1–65 Ma) is seen in figure 3. On the right-hand-side of this figure we permit approximately 90% of the total near-axial hydrothermal heat flux to be expressed in the form of low temperature flow, and 10% in the form of high temperature (i.e. 'smoker') flow. This division is in rough agreement with observations of seafloor hydrothermal systems (Schultz *et al.* 1992; Rona & Trivett 1992). We shall make use of this subsequently in calculating total global water fluxes. A theoretical underpinning for the generation of diffuse flow within high temperature hydrothermal systems is given later in this paper.

(*c*) *Magmatic budget*

An independent method of bounding the global hydrothermal heat budget comes from consideration of the total volume of new magma emplaced annually along the global ridge system. Kadko *et al.* (1994) and Elderfield & Schultz (1996) considered the latent heat of crystallization of basaltic magma (*ca.* 0.676 × 10^6 J kg^{-1}) which takes place at temperatures near 1200 °C, and then the residual heat of cooling the

newly crystallized rock from these temperatures to the temperatures of the fluids found to exit from high temperature hydrothermal vents (1.130 MJ kg^{-1} for cooling from 1200 to 350 °C typical black smoker vent temperature).

It may be argued that a more appropriate temperature for hydrothermal endmember fluids at the reaction zone (typically 2 km below seafloor) would either be 465 °C, i.e. by extrapolating surface hydrothermal temperatures adiabatically to the reaction zone, or even as high as 600 °C, (Morton & Sleep 1985; Phipps Morgan & Chen 1993). We shall therefore take 350 °C as a lower bound on the temperature (i.e. the upper bound on the hydrothermal component of lithospheric cooling), and 600 °C as an upper bound.

The total heat available for hydrothermal circulation based entirely on cooling magma from liquidus temperatures to the temperature of vent fluids is therefore 1.806 MJ kg^{-1} (Kadko *et al.* 1994). We compare this to the heat required to elevate a given mass of seawater at 2 °C (typical benthic temperature) to hydrothermal temperatures, or 350 °C. This is of course dependent upon depth, e.g. pressure. We expect a balance between magmatic cooling and seawater heating, since in the area of 'active' hydrothermal circulation, it is cooling of the magmatic intrusions by heating of seawater which leads to the production of high temperature endmember hydrothermal effluent. We have already concluded from the thermal models that conductive cooling in the near-axial zone contributes only a small part to the total cooling budget.

Bischoff & Rosenbauer (1985) have investigated the equation of state for a hydrothermal fluid analogue, i.e. 3.2% NaCl seawater by determining experimentally the pressure dependence of the specific volume of seawater. Temperatures of the isotherms were then fit to a compressibility equation, and an empirical equation of state was determined that relates the specific volume, compressibility and expansivity of seawater to the temperature and pressure.

For typical high temperature vent fluid exit temperatures of 350 °C, and for a typical depth of medium and fast-spreading mid-ocean ridges, i.e. 2500 mbsl, Bischoff & Rosenbauer's relationship shows the heat capacity of the hydrothermal fluids is approximately 6.5×10^{-3} MJ $kg^{-1}K^{-1}$ (figure 4). There is a complication in that values of the specific heat come close to the two-phase boundary, particularly near the critical point of *ca.* 405 °C and 300 bar where values of specific heat are known only approximately.

There is petrological evidence from fluid inclusions and from chemical analysis of quartz-cemented breccias (Delaney *et al.* 1987), and from direct measurements of high temperature vent fluid at the Juan de Fuca Ridge (Butterfield *et al.* 1994) that phase separation has been observed within certain hydrothermal systems. Butterfield & Massoth (1994) report on significant temporal variation of vent chemistry at the North Cleft segment of the Juan de Fuca Ridge between 1988 and 1992, suggesting transition from vapour-enriched to brine-enriched effluent during the course of volcanic activity. This is in general agreement with the Edmonds & Edmond (1995) model of mixing of phase-separated brine, vapour and hydrothermally altered seawater within the hydrothermal system, which in turn is consistent with Bishoff & Rosenbauer's (1989) double-diffuse convection model of the reaction zone. Phase separation effects will be considered later.

To heat 1 kg of seawater at 2 °C to 350 °C therefore is equivalent to *ca.* 2.262 MJ. The amount of heat released in cooling 1 kg of 1200 °C magma to 350 °C (which we presume is due to hydrothermal processes) is in the ratio of 1806/2262 the amount of

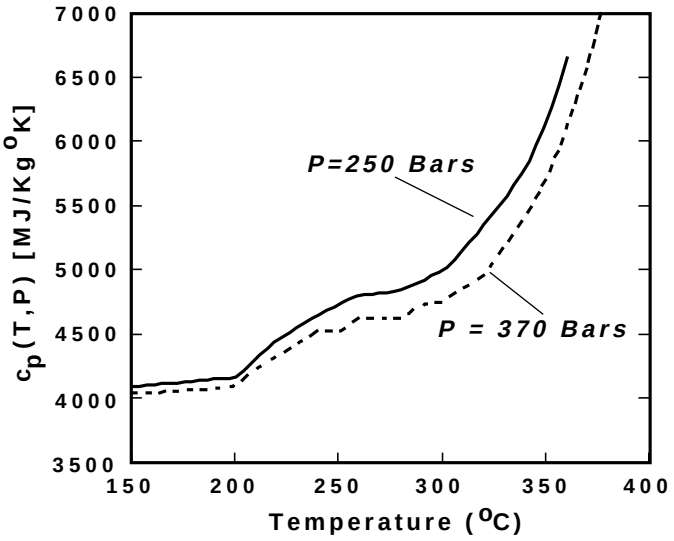

Figure 4. Specific heat of seawater *vs* temperature (°C) at 250 bar (solid curve) and 370 bar (dashed curve) pressure, roughly equivalent in the first case to the ambient seafloor hydrostatic pressure at vent fields throughout the East Pacific Rise and Juan de Fuca Ridge, and in the second to that at the TAG hydrothermal mound, Mid-Atlantic Ridge. The values shown have been interpolated from those found in Bishoff & Rosenbauer (1984).

heat necessary to heat 1 kg of ambient seawater to 350 °C; i.e. the heat liberated by cooling 1 kg of magma is sufficient to heat 798 g of water. Of greater interest perhaps is determination of the relative volume of magma involved in heating the equivalent volume of water. It is also of interest to compare the estimates of the total heat available to drive hydrothermal circulation determined from the mismatch between the Stein *et al.* (1995) lithospheric cooling model and observed heat flow, and the budget as estimated from the heat content of newly emplaced magma, integrated over the global ridge crest system.

Given a total volume of newly emplaced magma of 17 $km^3\,yr^{-1}$, and taking the density of seafloor basalt to be *ca.* 3000 $kg\,m^{-3}$, the total mass-per-year of newly emplaced magma is 5.1×10^{13} $kg\,yr^{-1}$. Given the figure above of 1.806 $MJ\,kg^{-1}$ liberated from cooling uncrystallized magma at 1200 °C to 350 °C, the total heat released by this process, globally, is 9.21×10^{19} $J\,yr^{-1}$, for a total heat flow of *ca.* 2.9×10^{12} W, or *ca.* 3 TW. This figure is in close agreement with that predicted by the mismatch between heat flow observations and the Stein & Stein (1994) and Stein *et al.* (1995) thermal models.

The estimated total heat budget can be more than doubled by increasing the reaction temperature from 350 °C to the upper bound of 600 °C. Even greater values are possible if the dramatic increase in c_p near the point of phase separation is taken into account. The aforementioned close agreement between the calculations appropriate for 350 °C with those obtained from the underlying thermal models suggests that this lower bound may be closer to the globally averaged truth, although locally there may be large variations from the global average.

Bishoff & Rosenbauer's calculations of specific volume for seawater at 250 bar and 350 °C yield a density of approximately 680 $kg\,m^{-3}$, compared with the density of ambient (*ca.* 2.7 °C) seawater at the same pressure of 1028 $kg\,m^{-3}$. In volumetric

terms therefore, the amount of heat released in cooling 1 m^3 of magma is sufficient to heat 3.52 m^3 of seawater. In mass heat exchange terms, the water/rock ratio for seafloor hydrothermal systems is nearly unity, while in volumetric terms it is about 3.5:1, i.e. each litre of magma will heat *ca.* 3.5 litres of high temperature hydrothermal effluent.

(*d*) *Global hydrothermal water budget*

Given knowledge of the specific heat of seawater under hydrothermal conditions, and given estimates of the total heat budget available to drive hydrothermal circulation through an area of seafloor at a particular temperature and pressure, it is possible to place bounds on the total volume of seawater necessary to transport that heat, i.e. the volume of seawater that must circulate through the global hydrothermal system each year. Such calculations are strongly parametric; they depend not only on the underlying thermal model (which we have seen is dependent itself on numerous assumptions), but also on estimates of the temperature to which those fluids are heated during their residence time within the lithosphere. Accurate estimation of the water budget would require full knowledge of the total path length over which the fluid circulates, and then integration of all pressure and temperature effects over that path length.

By ignoring considerations of variable P–T conditions over the path-length of the flow, one can transform the known quantities into water mass flux,

$$Q_{\mathrm{m}} = \frac{Q_{\mathrm{a}}}{\Delta T c_{\mathrm{p}}}, \tag{2.18}$$

where Q_{m} is the water mass flux (kg yr^{-1}), Q_{a} is the heat flux (TW), and ΔT is the temperature by which the ambient seawater is raised during its circulation within the lithosphere. An example of this naive means of calculating the global water flux is seen in figure 5. Here we have assumed that all of the axial hydrothermal heat flux is removed by hydrothermal flow at 350 °C, and that these fluids are heated at a depth equivalent to 250 bar. We assume further that all off-axis flow takes place at 5 °C and 250 bar. This ignores entirely the partitioning, on-axis, between high and low temperature flow, and also ignores the details of the reaction zone depths, the integrated path lengths of fluid flow, and seafloor bathymetric effects off-axis. The total water flux due to off-axis flow for lithospheric ages of 1–65 Ma (taken to be uniformly 5 °C above ambient temperatures) is 2.4×10^{16} kg yr^{-1}, while that due to high temperature axial flow within ages 0–1 Ma (uniformly 350 °C) is 2.4×10^{13} kg yr^{-1}.

(i) *Temperature and pressure effects on water volume calculations*

The accuracy of these estimates depends greatly on the underlying assumption that on average this circulation results in heating of seawater by 5 °C above ambient temperatures during the time it is resident within the lithosphere. This is an arbitrary assumption, and it may equally well be that most of the circulation takes place at cooler temperatures. It seems certain that the bulk of off-axis flow takes place at temperatures below 30 °C (Honnorez 1981; Gallahan & Duncan 1994) but the lower bound on, and spatial distribution of off-axis upper lithospheric temperatures are as yet constrained poorly. The effect of this would be that the total transport of seawater into the lithosphere would scale, almost linearly at these temperatures, with the reciprocal temperature increase above ambient.

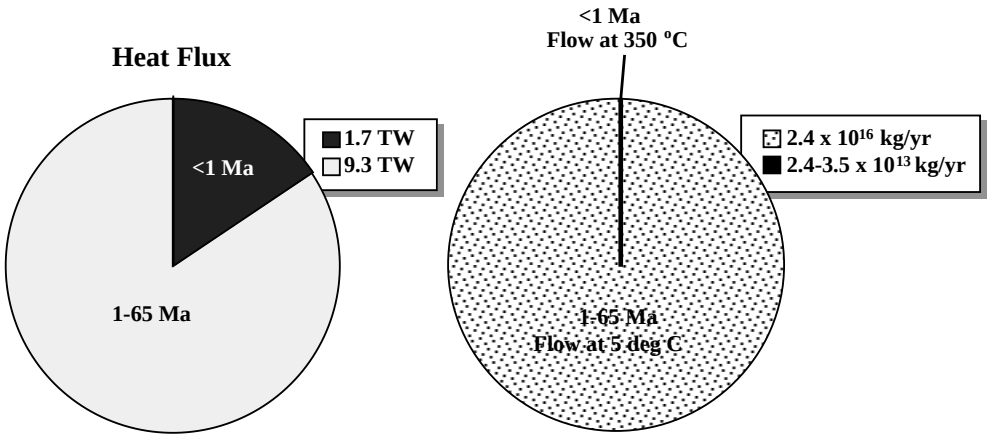

Figure 5. Total budget of hydrothermal fluids circulating through the oceanic lithosphere. The heat flux which drives the circulation (left). The mass of water necessary to cool the lithosphere, divided into axial (0–1 Ma) and off-axis (1–65 Ma) components (right). The axial component is calculated by making two different assumptions (described in the text), leading to a 46% difference in the estimates of total water circulation.

The effects of variable temperature on the specific heat of seawater may be taken into account by integrating with respect to temperature the relationship between specific heat and volume flux,

$$Q_{\mathrm{m}} = Q_{\mathrm{a}} \Big/ \int_{2\,^{\circ}\mathrm{C}}^{350\,^{\circ}\mathrm{C}} c_{\mathrm{p}}(P,T)\,\mathrm{d}T. \tag{2.19}$$

If we consider that the fluid has been heated at a constant pressure of 250 bar, the water volume flux, integrating over all temperatures from 2 to 350 °C becomes 3.5×10^{13} kg yr^{-1}, an increase of 46% over the more naive estimate above.

The effects of pressure on c_{p} of seawater are less than, and act in opposition to, those due to temperature (Bischoff & Rosenbauer 1984; and figure 4). The total water budget due to high temperature flow shall increase somewhat, but proportionally less so, if the integral in the equation above were replaced by a double integral taking the pressure dependence into account. By extrapolating from the results of Bischoff & Rosenbauer we find that at 350 °C the value of c_{p} decreases by *ca.* 15% at 450 bar relative to that at 250 bar, which is equivalent to the presumed depth of the reaction zone beneath a typical medium or fast-spreading ridge crest. The effects on the total water budget attributed to high temperature axial flow, integrated over the path length of that flow, will be commensurately smaller than this adjustment. We may therefore discount pressure dependence as falling well within the accumulated errors in these calculations and elect to consider only the single integral form of (2.19).

The major impact of pressure on calculations of heat flux stems from the potential for phase separation of the fluids. By increasing pressure at a given temperature such that the P–T regime falls below the critical point of phase separation, c_{p} decreases dramatically. The heat content of a given volume of hydrothermal fluid would drop significantly relative to fluids of the same T but somewhat lower P which fall on the other side of the critical point.

Pressure dependence of c_{p} would have essentially no effect on lower-temperature axial diffuse flow and off-axis flow as c_{p} achieves a nearly constant (pressure-independent) value for temperatures below *ca.* 200 °C.

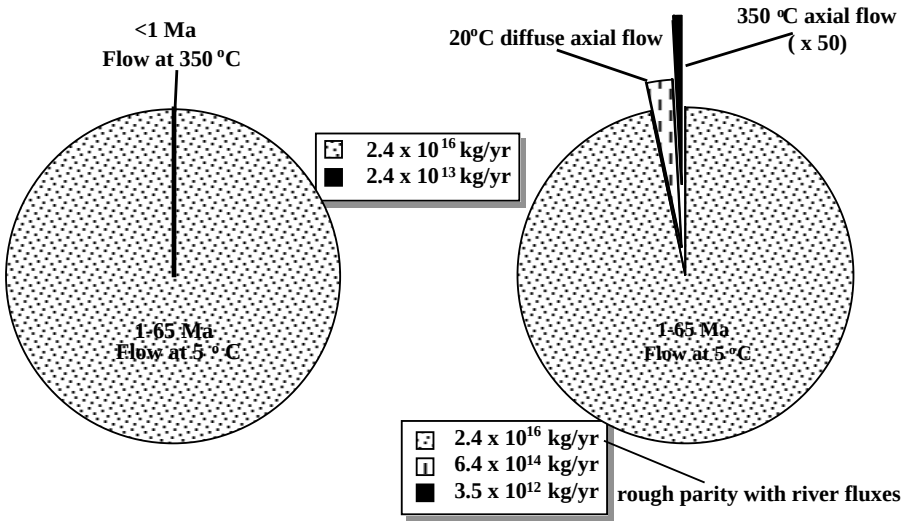

Figure 6. Total budget of hydrothermal fluids circulating through the oceanic lithosphere. The heat flux which drives the circulation (left). The mass of water necessary to cool the lithosphere, divided into axial (0–1 Ma) and off-axis (1–65 Ma) components (right). The axial component is calculated by presuming that 10% of the flow takes place at 350 °C, and 90% at 20 °C.

If we take the conservative view in terms of total volume of water transported that temperatures are raised 5 °C above ambient, we see that on average the equivalent of about 1 Sv (Sverdrup, or 10^6 m^3 s^{-1}) of seawater is transported through the lithosphere by hydrothermal circulation. This is approximately 1/30th of the total transport of seawater through the Gulf Stream, and in rough parity with the total flux of river water entering the world oceans (Elderfield & Schultz 1996).

Given the three-orders-of-magnitude difference in apparent water budgets associated with axial and off-axis regimes, the axial component of flow appears of little consequence to the total global water budget. This is in stark contrast to the impact of the high temperature axial component of seafloor hydrothermal flow on ocean chemistry. Although flank flow systems are quantified only poorly, the current evidence is that high temperature flow is by far the dominant hydrothermal contributor of both sources and sinks to global ocean chemistry (Elderfield & Schultz 1996). Furthermore, if one considers the contributions of lower temperature diffuse axial flow to the heat budgets, it becomes apparent that the associated water budgets increase dramatically.

We take the heat flux values presented in figure 3, accommodating axial diffuse heat flow in the ratio of 10:1 with axial high temperature flow, and convert these into water fluxes (equation (2.19)). This is seen in figure 6. The total axial flow due to diffuse modes, assuming these take place uniformly at a temperature elevated 20 °C above ambient, is 6.4×10^{14} kg yr^{-1}, or roughly 3% of that associated with low temperature off-axis flow. The corresponding water budget due to high temperature 350 °C flow drops to 3.5×10^{12} kg yr^{-1}. While still a small percentage of the total water circulating through the oceanic lithosphere, axial diffuse flow takes place at higher temperatures, and as seen later, is involved in considerable chemical exchange with the oceanic lithosphere and oceans.

3. Diffuse flow is an intrinsic feature of high temperature flow

A theoretical and observational framework has been provided showing that hydrothermal circulation persists throughout the oceanic lithosphere to ages as great as 65 ± 10 Ma. We consider in this section the nature of hydrothermal circulation in the youngest, hottest part of that system, the axial region (0–1 Ma). On axis, hydrothermal circulation may be modelled as that due to flow within a highly cracked permeable medium. Cracks within the sheeted dyke complex and extending up into the pillow basalt layer likely provide the predominate pathways by which fluids heated at the reaction zone are transported rapidly up to the seafloor.

Within the permeable subdomains in this region fluid flow is governed by D'arcy's Law which describes the relationship between the pressure gradient driving the flow with a given velocity and the opposing viscous forces,

$$\bar{u} = -\frac{k}{\mu}(\nabla P + \Delta\rho g\hat{z}), \tag{3.1}$$

where $\bar{u} = (\hat{x}u + \hat{z}w)$ is the transport velocity in Cartesian coordinates $(\hat{x}, \hat{z})$, k is the permeability of the medium, μ is the dynamic viscosity of fluids within the medium, P is the pressure, $\Delta\rho$ is the density difference determined by the temperature distribution, and g is gravitational acceleration (Phillips 1991). For D'arcy flow in a two-dimensional medium with isotropic permeability the resulting equations are,

$$\left.\begin{aligned} \frac{\partial^2 p}{\partial x^2} + \frac{\partial^2 p}{\partial z^2} &= \rho_0 \alpha g \frac{\partial T}{\partial z}, \\ \frac{\partial^2 \Psi}{\partial x^2} + \frac{\partial^2 \Psi}{\partial z^2} &= -\frac{\rho_0 k \alpha g}{\mu}\frac{\partial T}{\partial x}, \\ \frac{\partial \Psi}{\partial z}\frac{\partial T}{\partial x} - \frac{\partial \Psi}{\partial x}\frac{\partial T}{\partial z} &= \kappa\left[\frac{\partial^2 T}{\partial x^2} + \frac{\partial^2 T}{\partial z^2}\right], \end{aligned}\right\} \tag{3.2}$$

where Ψ is the stream function field and α is the coefficient of thermal expansion.

While appropriate for defining the flow and temperature fields within any given permeable region, this formulation is inappropriate to describe the flow within a crack bounding such a region. We consider flow within a crack to be represented by turbulent pipe flow which obeys the relationship

$$\frac{\partial p}{\partial z} = \frac{\rho_{\mathrm{i}} f v_{\mathrm{f}}^2}{4a_{\mathrm{p}}}, \tag{3.3}$$

where ρ_{i} is the density of the fluid in the pipe, f is an empirical friction factor, v_{f} is the turbulent fluid velocity, and a_{p} is the radius of the pipe (Turner & Campbell 1987).

(a) *A model of flow within a cracked permeable domain*

We take a model (figure 7) of a permeable medium surrounding a pipelike crack to represent a high temperature fluid source, originating at depth within the seafloor and communicating with the reaction zone deep within the hydrothermal system. The crack is embedded within the permeable seafloor and acts to channel high temperature fluids from the source and up into the water column. On a finer scale, such a model might also serve to represent the flow within an individual hydrothermal edifice.

In order to solve equations (3.1) and (3.2) for the given geometry we set the

following boundary conditions. The temperature at the base of the structure ($z = L/2$) is set to a constant 360 °C at the origin, and extending along the bottom a distance $L/2$ from that point. The temperature then decreases exponentially from that point such that $T = 0$ at $x = L$. The origin is the centreline of the vertical pipe, and the model is two dimensional and symmetric about that axis.

The temperature of the pipe wall is set to 360 °C isothermally, which we take to be the temperature of the 'black smoker' source fluids flowing upward through the pipe. The pipe wall is made permeable such that hydrothermal source fluids may seep into the surrounding region and mix there with seawater advected into the structure. The advection takes place in response to the lateral pressure gradients set up within the permeable medium in response to the vertical flow within the pipe.

Variable boundary conditions are set at the top of the permeable subdomain. In locations where the solution requires effluent to flow outward from the structure, we require the vertical gradient of temperature at the seafloor–ocean interface (i.e. the heat flux due to thermal conduction) to be zero. In locations where the solution requires advection of cool seawater into the top of the permeable region, we require the temperature (rather than its vertical gradient) at that boundary to be zero. Thus, we alternate between Dirichlet and Neumann conditions depending upon the local behaviour of the solution.

For the model shown in figure 7, the geometry represents a permeable block with sides elevated above that of the surrounding seafloor, following Schultz *et al.* (1992). In this case, the boundary conditions along the side at $x = L$ are equivalent to those at the top, i.e. zero horizontal temperature gradient for zones where effluent flows outward from the sides of the structure, and zero temperature for zones where cool seawater is advected into the structure. We permit no vertical component to the effluent velocity at this boundary, thus $\Psi_x = 0$.

The top panel of figure 7 is diagnostic. The stream function field reveals the pattern of seepage into the structure of hydrothermal source fluids from within the pipe. There are strong horizontal gradients in Ψ extending from the origin to nearly $x = L/2$, at which point the horizontal gradient drops precipitously. The vertical velocity of the effluent flowing within the permeable medium is derived from the horizontal gradient of the stream function, thus near $x = L/2$ the upward flow of effluent out of the structure ends, and a broader zone of much slower flow of seawater into the top and sides of the structure begins. Within the upflow zone in the part of the structure near the origin ($x < L/2$), the strong lateral gradient in Ψ indicates there is a rapid drop-off in vertical effluent velocity as one moves away from the origin (i.e. the 'pipe' or plume feeder source).

The part of the mound centred around $x = L/2$ is a zone of intense mixing between in-flowing seawater and out-flowing effluent. There is a notable vertical gradient in Ψ, associated with a significant horizontal component to flow of effluent within the structure seen in the bottom right-hand quadrant of the top panel of figure 7. This indicates there is a preferential band of in-flow along the thermal boundary layer that has formed (this is seen clearly in the bottom panel, i.e. the temperature field).

The relationship between the permeability of the structure and the temperature and velocity fields observed at the top boundary is shown in figure 9. Here three different sets of solutions to (3.1) and (3.2) are presented for the geometry shown previously in figure 7. Each solution corresponds to the identical geometry but a different isotropic permeability, and thus a different Rayleigh number. In the first instance, for the geometry shown and for permeabilities no greater than 10^{-12} m^{-2},

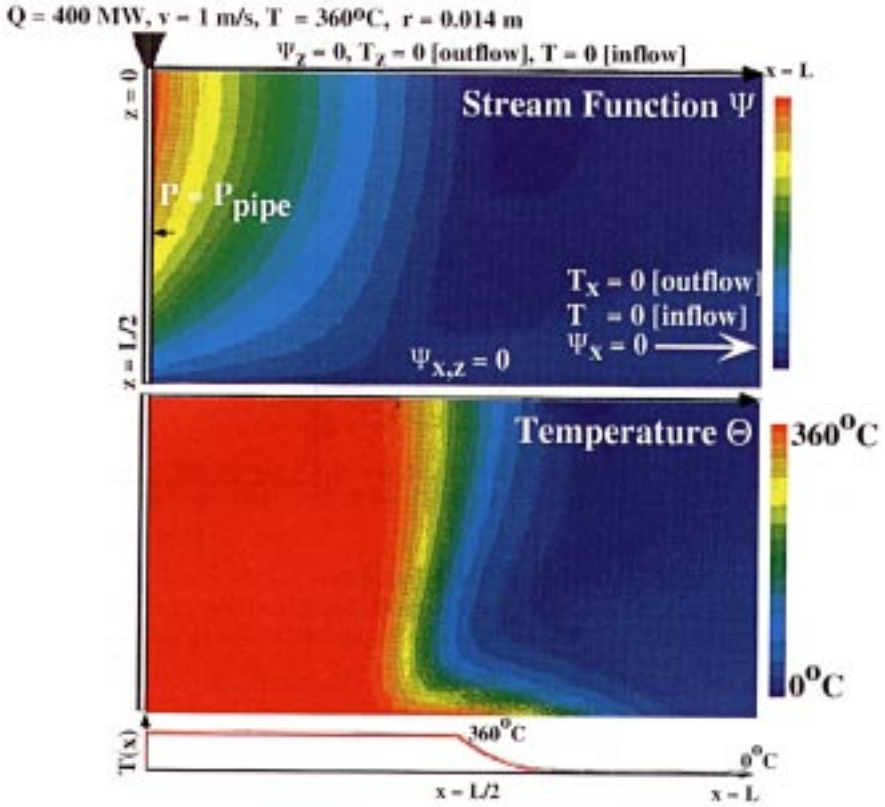

Figure 7. Solution for temperature and stream function fields within a two-dimensional permeable block with embedded crack. The flow within the crack, located at the axis of symmetry of this model, is taken to obey laminar pipe flow law. Solution by P. Dickson using a sparse iterative steady-state finite difference solver modified from Dickson *et al.* (1995).

the solution for D'arcy flow simplifies to that of a diffusion equation, i.e. advection terms become unimportant and the Rayleigh number becomes small. At the highest permeability shown, $k = 10^{-11}$ m^{-2}, the Rayleigh number increases and the effluent vertical exit velocity at the top boundary rises sharply (right panel of figure 9). The isotherms move inward toward the origin (left panel) as the effect of the cool advected seawater on the periphery of the structure is observed. For structures of different geometry the permeability at which advection will dominate over diffusion will differ from that found for this particular case, but there will exist a range of parameters for which solutions of this sort hold.

It is possible to obtain a stable numerical solution for D'arcy flow for the present geometry and using the sparse iterative finite difference solution employed here (Dickson *et al.* 1995) only for low permeability. At higher permeabilities, the D'arcy assumption of a balance between pressure gradients and viscous drag begins to reach a limiting case and it becomes impossible to drive fluid more quickly through the permeable region. In the true seafloor system it is likely that flow is instead dominated by the presence of small-scale cracks which provide highly permeable pathways in which higher velocity pipe flow, sheet flow, or other modes prevail, and in which D'arcy flow is not appropriate. In the area immediately surrounding each of these small permeable pathways however, D'arcy flow would hold locally, and the effects seen in figure 9 would, under the appropriate range of conditions, appear.

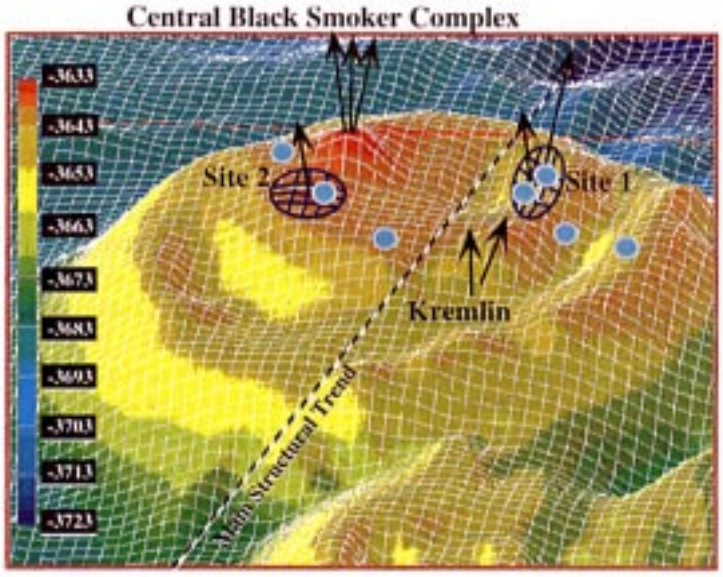

Figure 8. Bathymetric map of TAG mound. Flow emanating from central black smoker complex and from individual high temperature venting sites likely results from fluids channelled upward into the mound via highly permeable cracks of the sort represented in figure 7. The colour scale indicates depth in metres, and the horizontal scale of the mound is *ca.* 200 m across. Bathymetric data are from AMS-120 sidescan sonar survey, courtesy of P. Shaw, M. Kleinrock and S. Humphris.

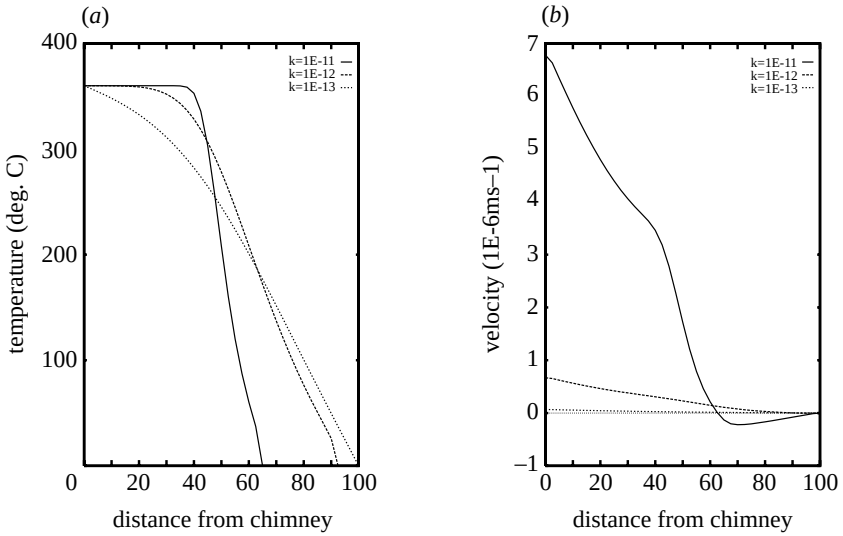

Figure 9. (*a*) Temperature in °C at the top surface (seafloor) of the two-dimensional permeable block *vs* horizontal distance in metres from the embedded crack for the model shown in the figure 7. (*b*) As (*a*), but vertical exit velocity of the hydrothermal effluent. Both (*a*) and (*b*) contain three sets of curves representing the flow solutions for permeabilities of $k = 10^{-11}$ m^{-2} (solid), 10^{-12} m^{-2} (long-dashed) and 10^{-13} m^{-2} (short-dashed) respectively.

In conclusion, figures 7 and 9 demonstrate the principle that in a crack-dominated system analogous to high temperature hydrothermal venting, there will exist a 'halo'

of lower velocity broad-scale diffuse hydrothermal efflux which arises as a passive and intrinsic feature of the faster source flow. Horizontal pressure gradients are set up within a permeable medium surrounding a crack through which fluids flow, and in response seawater is entrained into such a body, mixes with the hydrothermal effluent entering the body from the walls of the source conduit, and then exits the top of the structure in a broad zone. We shall consider in the following section aspects of the chemical interactions that take place between the rocks making up the permeable region and the mixture of hydrothermal effluent and seawater flowing within it.

4. Combined chemical and physical measurements of diffuse effluent

One of the most important sets of measurements on submarine hydrothermal systems is those that characterize the fluxes of heat, water and chemical constituents and determine how they vary spatially and temporally. Because of the coupling of heat and chemical fluxes, these estimates are essential to determine the impact of hydrothermal systems on ocean chemistry (Elderfield & Schultz 1996). In this, we must recognize that high-temperature ('black smoker') flow and lower-temperature ('white smoker') and diffuse flow all must be sampled. Most work has emphasized the more spectacular high-temperature parts of hydrothermal systems. However, experiments to quantify the balance between diffuse (low temperature) and discrete (high temperature) sources on the Juan de Fuca Ridge (Schultz *et al.* 1992) have suggested that discrete flow only accounts for 1/5th to 1/10th of the axial heat flow. Thus, determination of the relative importance of these two flow paths is vital.

Rudnicki & Elderfield (1992) calculated a total thermal flux of 500–900 MW for the TAG vent field from plume data, a figure which compares with 120 MW for the main black smoker venting complex at the summit of the TAG mound (Rona *et al.* 1990). This indicates that possibly 3/4 to 6/7th of the total TAG hydrothermal mound heat flux derives from low temperature systems which are entrained into the plume. This does not take into account diffuse flow that is not entrained in plumes, a discussion of which appears later.

(*a*) *Diffuse effluent chemistry*

The documentation of the chemistry of the on-axis diffuse flow is extremely poor. It relies principally on inferences based on the composition of hot spring deposits (Alt *et al.* 1987) and efforts to sample diffuse fluids directly by our group and by a few others (Butterfield & Massoth 1994). Recently, Mills *et al.* (1993) have provided some evidence of diffuse fluid chemistry from analyses of pore waters from metalliferous sediments at TAG but the only lower temperature fluids which had previously been sampled directly at TAG were 'white smokers', from a small cluster of sphalerite-rich dome structures to the southeast of the mound (the 'Kremlin' area *ca.* 50 m S of 'Site 1' in figure 8), and comprise *ca.* 15% seawater and *ca.* 85% high-temperature hydrothermal fluid with exit temperatures of *ca.* 300 °C (Edmond *et al.* 1995). However, diffuse flow of low-temperature fluids is ubiquitous over the top and sides of the mound, and is potentially of greater importance for the formation of ore deposits.

The development of the 'Medusa' system for sampling diffuse hydrothermal effluent and measuring its physical properties in situ (Schultz *et al.* 1996) enabled in 1994 and 1995 the first direct sampling of diffuse effluent exiting the TAG mound. The time series records and chemical samples discussed here were obtained from a

Table 2. *TAG fluid compositions*

(Composition of black smoker, white smoker and diffuse flow fluids from TAG, extrapolated to Mg = 0 (data from Edmond *et al.* (1995) and James (1995)).)

element	black smoker	white smoker	diffuse flow
Li (μM)	411	383	366
Rb (μM)	9.1	9.4	9
Ca (mmol kg^{-1})	0.8	27	22
Sr (μmol kg^{-1})	103	91	71
$^{87}Sr/^{86}Sr$	0.7038	0.7046	0.70304
pH	3.35	3	—
H_2S (mM)	2.5-3.5	0.5	< 0.04
Si (mM)	20.75	19.1	17
Cl (mM)	636	—	640
Fe (μM)	5590	3830	3260
Mn (μM)	680	750	635
Zn (μM)	46	300–400	62
Cu (μM)	120–150	3	< 3
La (pmol kg^{-1})	3710–4610	3590	2810
Ce (pmol kg^{-1})	8820–10200	4360	6970
Nd (pmol kg^{-1})	5250–6990	1590	4460
Sm (pmol kg^{-1})	1040–1450	250	920
Eu (pmol kg^{-1})	3390–3690	13800	9710
Gd (pmol kg^{-1})	895–1330	160	838
Dy (pmol kg^{-1})	635–907	110	528
Er (pmol kg^{-1})	281–336	46	203
Yb (pmol kg^{-1})	169–249	46	182
Lu (pmol kg^{-1})	21.4–30.6	4	24

'Medusa' system deployed at 'Site 1' for a period of six months in 1994–1995. Spot measurements of diffuse effluent velocity and temperature were obtained from broad areas of the mound from sites representative of the diffuse flow regime found in the given areas. Concurrent samples of diffuse flow chemistry were obtained from seven sites on the mound (marked in figure 8 by filled cyan-coloured circles).

There appear to be two main venting centres on the mound. The first is the central black smoker complex, the trend of which continues southward to 'Site 2' (figure 8). The second is a feature extending from 'Site 1' along the trend of a grabenlike feature orientated NE–SW, and then south to the 'Kremlin' area. Areas of extensive black smoker flow are indicated on the figure by black arrows.

For comparative purposes with TAG black smoker (mainly from the central black smoker complex) and white smoker fluids (from the 'Kremlin' area), the concentration data for the diffuse flow (from the points marked on figure 8) have been extrapolated to zero Mg in table 1.

Data for several species (e.g. Li, Mn, Cl and Rb) in the diffuse flow fluids is best described as a mixture of high-temperature ('black smoker') fluid and seawater. This

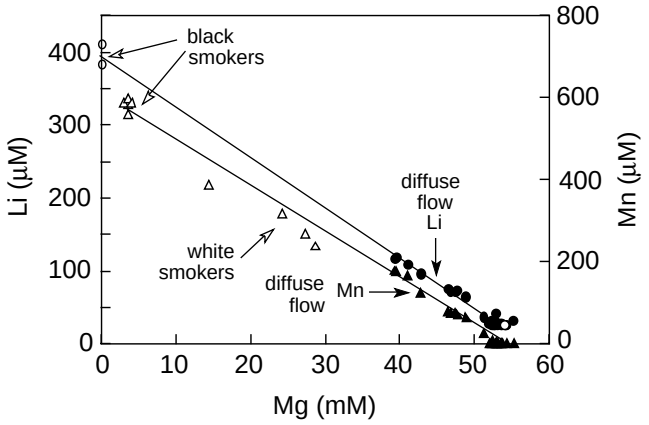

Figure 10. Li and Mn versus Mg in diffuse hydrothermal fluids at TAG. Also shown are compositions of black and white smoker fluids.

is shown in figure 10 using Mg as an index of seawater and implies that these species behave conservatively throughout the subsurface mixing process.

However, concentrations of other elements in the diffuse flow fluids are not conservative (figure 11). Fe in the diffuse flow endmember is *ca.* 44% depleted relative to that in black smoker fluids and H_2S is below the limits of detection. Si is also depressed by 20%, and Ca and Sr by 30%, relative to black smoker fluids. This is due to the precipitation of Fe-sulphides, silica and anhydrite as the high-temperature fluids mix with seawater within the mound. ODP drilling has shown that these three phases are commonly found within the interior of the TAG mound (Humphris *et al.* 1996). Thus, the fluid chemistry demonstrates the active precipitation of the three principal mineral types found at TAG as a consequence of mixing of entrained seawater with high temperature black smoker fluids, as expected by the flow simulation seen previously in figure 7.

Another group of elements, including Cu, Zn, REEs and U, show complex behaviours as a result of their migration within the mound by the process known as 'zone refining' (Franklin *et al.* 1981; Edmond *et al.* 1995) and this is described in detail by James (1995) and James & Elderfield (1996).

Because the chemical anomalies in the diffuse fluids attributable to precipitation of sulphide, anhydrite and silica within the hydrothermal deposit are known (figure 11), it is possible to estimate the rates of deposition of these minerals as a function of heat flux (figure 12). The formation rate (R) is given simply by

$$R = \frac{\Delta M Q_{\mathrm{a}}}{c_{\mathrm{p}} T_{\mathrm{p}}}, \tag{4.1}$$

where ΔM is the concentration difference between the diffuse flow endmember and the black smoker endmember at zero Mg, Q_{a} is the (advective) heat flux, and T_{p} is the temperature of mineral precipitation.

In this case, we define 'diffuse endmember' as the product of high temperature hydrothermal effluent that has mixed internally with seawater entrained into the interior of the mound, and which has reacted within the interior with the minerals making up the fabric of the mound. We do not refer here to high temperature effluent that has been diluted with seawater within the near-bottom water column. The

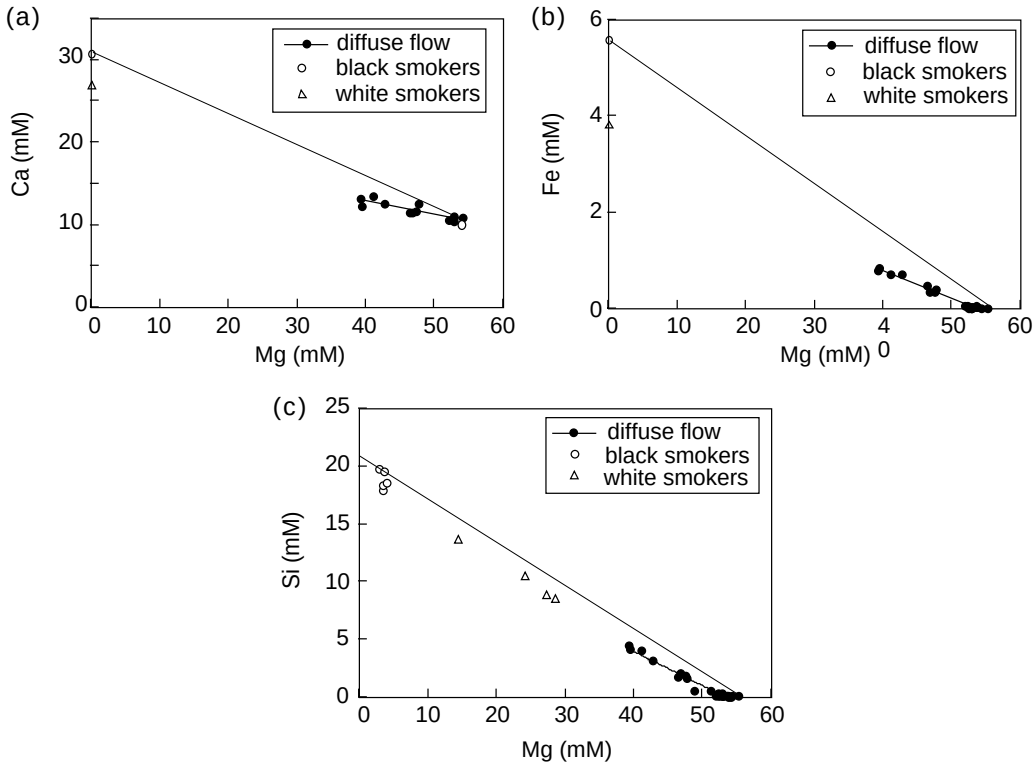

Figure 11. (*a*) Ca versus Mg, (*b*) Fe versus Mg, and (*c*) Si versus Mg in diffuse hydrothermal fluids at TAG. Also shown are compositions of black and white smoker fluids.

'Medusa' sampling system has been designed specifically to inhibit such dilution and thus to maximize the probability of obtaining uncontaminated diffuse endmember fluids. We consider this a prerequisite for accurate analysis of the chemical signature of both high and low temperature water–rock interactions.

From these estimates of R, the time taken (τ) for the mound to have attained its current inventory (A) of minerals (Tivey *et al.* 1996) can be estimated, thus providing an index of preservation (figure 13*b*):

$$\tau = A/R. \tag{4.2}$$

(i) *Areal measurement of heat flux density and the longevity of the TAG system*

A series of 'Medusa' spot measurements of effluent temperature and velocity were taken over the surface of the TAG mound (e.g. figures 8 and 12).

Each cluster of points in figure 12 represents a single sampling episode where the manned submersible used to position the instrument has removed the instrument's sensor head (Schultz *et al.* 1996) from the submersible's instrument basket and placed it directly atop diffuse flow emanating from the seafloor (in this case a surface of sulphide rubble atop the TAG mound). A single sampling episode lasts approximately 5–10 min, during which time there are continuous measurements made of effluent and ambient seawater temperature and vertical effluent velocity. (Transmissometry has recently been added to the capabilities of the instruments.) The gaps between clusters

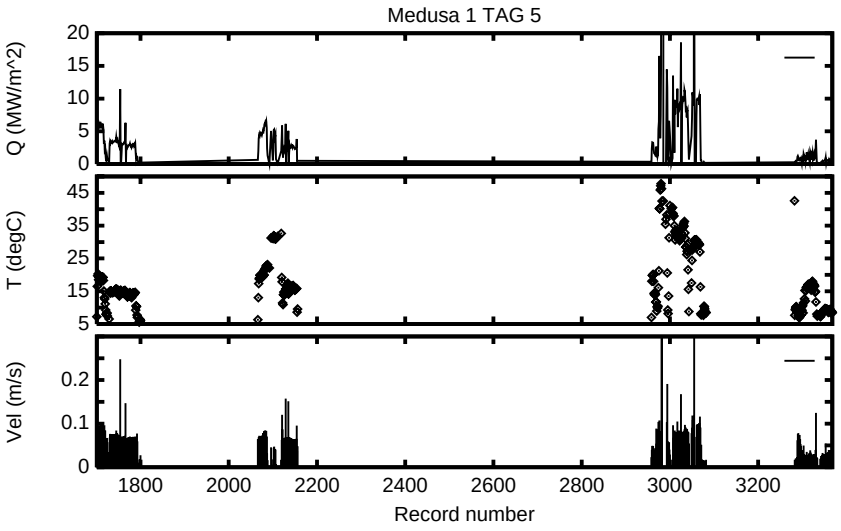

Figure 12. Typical spot measurements of diffuse effluent velocity, temperature and heat flux density taken at four closely spaced locations on the TAG mound (these sample locations are marked by filled circles in figure 8) using the 'Medusa' sampling system.

of points represent time periods where the submersible has replaced the sensor head in the instrument basket, and is traversing the surface of the mound en route to the next sampling location. At each sampling location it is possible to trigger any of a set of six 170 ml titanium syringe sample bottles which draw effluent from the interior of the sensor head, thus providing a means of concurrent sampling of the physical parameters and chemistry discussed within this section.

From the suite of spot measurements, the heat flux density over areas of the mound associated with visible diffuse efflux has been estimated as 2.5–8 MW m^{-2}. We observe diffuse flow of this magnitude over at least 1% of the total surface area of the mound. Over large areas of the remainder of the mound from which there is no visual indication of diffuse efflux, conductive heat flow measurements reveal vertical temperature profiles that are consistent with conductive rather than advective cooling (Becker & Von Herzen 1996). Over the remainder of the mound, diffuse advective discharge may exist, but below the limits of visual detectability, and also below the sensitivity threshold of the present configuration of our measurement system (i.e. very much less than 1.0 mm s^{-1}).

A lower bound on the total heat flux due to diffuse flow is therefore 780–2513 MW, based only on areas over which there is visible efflux, which suggests that the diffuse heat flux is roughly (and conservatively) an order of magnitude greater than the high-temperature heat flux of 120 MW. The mean and upper limit of this bound exceeds the upper limit of the Rudnicki & Elderfield (1992) estimate of 500–900 MW for the TAG vent field from plume data. This may be indicative of a part of the diffuse flow that is not entrained into the buoyant plume originating in the high temperature vent systems within TAG, and thus unaccounted for by measurements taken exclusively in the water column at the presumed height of neutral buoyancy of the main plume (i.e. *ca.* 200–300 m).

Anhydrite precipitates up to an order of magnitude more rapidly than sulphides and silica. Taking a figure of 2000 MW as that due to diffuse flow, mineral precip-

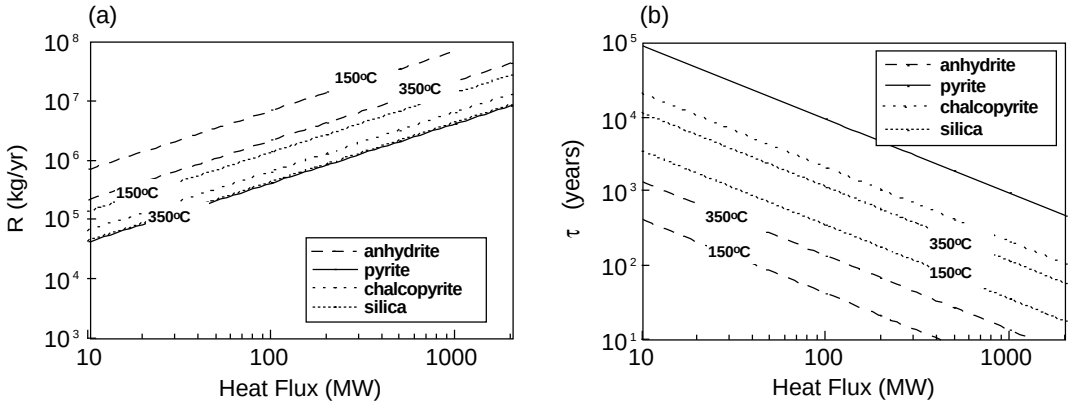

Figure 13. (*a*) Precipitation rate of various minerals versus heat flux attributed to diffuse flow, and (*b*) time taken for TAG mound to attain its current inventory of minerals. Based on James (1995), James & Elderfield (1996) and Tivey *et al.* (1995).

itation rates are of the order of 10^6–10^7 kg yr^{-1} of sulphide and silica and about 5–15 $\times$ 10^7 kg yr^{-1} of anhydrite.

According to Lalou *et al.* (1990), the TAG mound has grown episodically over the last 20 000 years and active hydrothermalism resumed about 50 years ago. On the basis of figure 13, it would seem that the mound anhydrite is contemporary, irrespective of choice of heat flux, and may represent as little as a few years of growth whereas mound sulphides and silica are clearly not contemporary, and represent 300–3000 years of growth. This is less than the age of the oldest hydrothermal deposits (20 000 years) and reflects, in part, periods where no mineral precipitation occurs and, in part, is indicative of reworking and oxidation of the sulphides.

5. Time series measurements at TAG

The spatial sampling of the physical and chemical properties of diffuse effluent at TAG has illustrated the range of contemporary mineralization processes taking place within this active hydrothermal system and has shed light on the episodic nature of hydrothermalism. Episodicity over tens to thousands of years is one extreme on the continuum of temporal variations in the hydrology of the system. The predominant modes of variability in the physical properties of diffuse effluent that we have observed over a six month instrument deployment period at TAG are those linked to tidal periodicities.

(*a*) *Previous observations of tidal variability*

Variations with tidal periods in both high temperature and low temperature flow have been observed for nearly a decade. Little *et al.* (1988) observed a strong semi-diurnal variation (peak-to-peak) of *ca.* 2 °C in temperatures measured over a twelve-day period a few centimetres above the seafloor in a diffuse flow area of the Guaymas Basin. This variation was taken to represent the modulation of the height of the near-bottom thermal boundary layer by tidal ocean currents (the modulation of tidal height at nearby Guaymas, Mexico is predominantly diurnal, thus the tidal (horizontal) speed variations are half this period, or semi-diurnal).

Schultz *et al.* (1992) analysed six weeks of continuous diffuse effluent and ambient temperature and diffuse effluent velocity data obtained in 1988 from the Endeavour Segment, Juan de Fuca Ridge. Here too, strong variations in temperature (several degrees peak-to-peak) with predominantly semi-diurnal periodicity were observed. In addition, a fixed array of ten thermocouples suspended directly above a high temperature smoker vent orifice detected strong semi-diurnal variability in black smoker plume temperatures (Monfort & Schultz 1988). The high temperature variability was interpreted as resulting from the lateral translation of the plume across the array of fixed temperature sensors as the plume was wafted back-and-forth by ocean tidal flow.

Another possible interpretation of the diffuse flow data was contamination of fluids entering the diffuse flow instrument (which in this case consisted of a vertical tube joined at the bottom to a funnel which was emplaced directly atop a percolating sulphide structure, and in which effluent velocity was detected by electromagnetic induction methods). In this instrument, the base of the flow-concentrator funnel was not sealed directly to the seafloor, making it possible for seawater to be advected into the base of the instrument where it would have the possibility to mix with diffuse endmember fluids. This advection could be modulated by the flow of tidal waters. Finally, it was considered that there may be pathways of sufficient permeability within the sulphide structure that broader tidal motions of the water column may be channelled into the interior of the structure and thereby modulate effluent temperatures.

(*b*) *Tidal variability at TAG*

Time series of diffuse effluent velocity and temperature, and the temperature of ambient seawater obtained during a $2\frac{3}{4}$ day period in September 1994 from 'Site 1' on the TAG mound (see figure 8) are shown in figure 14. The thicker curves represent low-pass filtered calibrated data (Schultz *et al.* 1996), using a robust moving average filter with 2 h corner period (Schultz *et al.* 1992). The thin curves represent the best fitting diurnal and semi-diurnal equilibrium tidal components (specifically the K_1, P_1, O_1, K_2, S_2, M_2 and N_2 lines). The tidal fits to these time series were obtained by calculating the discrete Fourier transform at these specific diurnal and semi-diurnal frequencies (Hendershott 1981), although the short duration of the time series section relative to the tidal periods makes it impossible to distinguish between the individual diurnal and semi-diurnal lines, rather only broad spectral peaks may be resolved.

Spectral resolution is illustrated in figure 15. Here the power spectrum for the diffuse effluent temperature was calculated by using the prolate taper function method of Thomson (1982) which was applied to a time series section spanning approximately two months in October–December 1994. The spectrum is plotted within an envelope representing ± 1 standard error. A number of distinct peaks are revealed showing that the effluent temperature is modulated primarily by semi-diurnal variations and harmonics, although there is significant power in the diurnal band, as well as even longer period variations extending to two days as well.

The undisturbed time series section is too short to show quantitatively that variations with periods greater than about two days exist. There was an episode of substantial disturbance to flow that is attributed to ODP drilling activities at TAG. The relationship between these activities, the effluent temperatures, and the penetration of specific anhydrite breccia petrological horizons is discussed in Schultz *et al.* (1996). These effects have limited our ability to resolve longer period natural

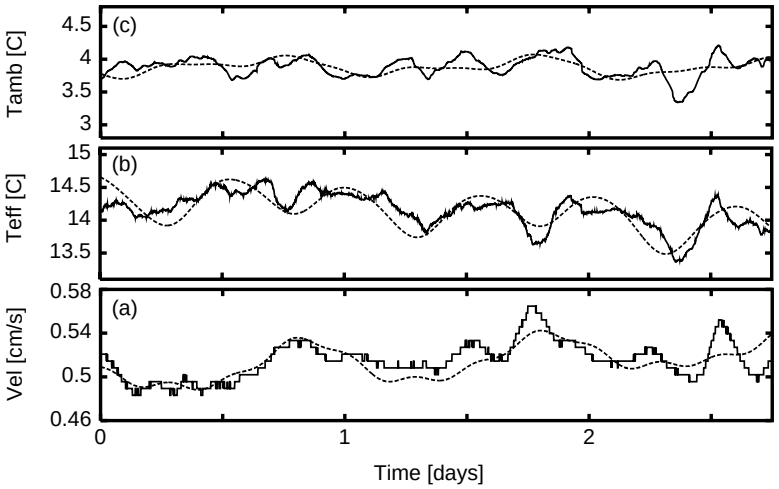

Figure 14. Time series of diffuse effluent (*a*) vertical exit velocity, (*b*) temperature, and (*c*) ambient seawater temperature measured by Medusa monitoring system 1 at TAG Site 1 for a three day period in 1994 before initiation of ODP drilling at TAG. The thin smooth curves are the time series obtained from the best-fitting diurnal and semi-diurnal tidal variations while the rougher curves are the actual measurements.

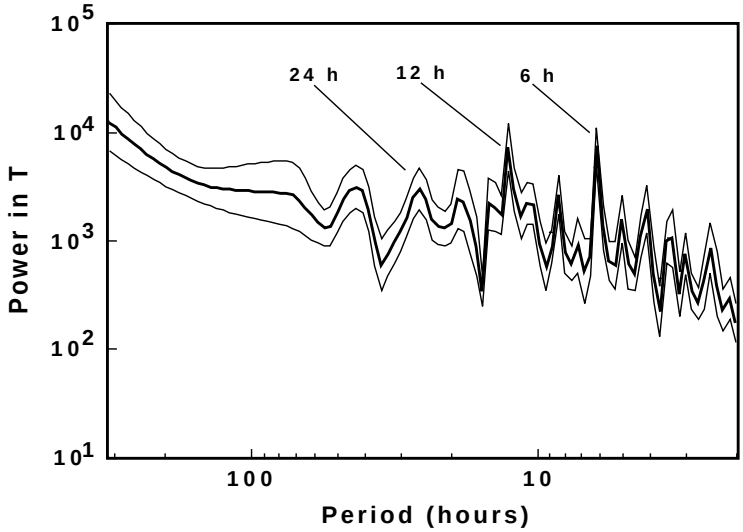

Figure 15. Power spectrum for diffuse hydrothermal effluent temperature variations as recorded as TAG Site 1 by Medusa 1 during the period 19 October to 25 December 1994. The spectrum shown is a robust estimate based on taking a series of 792-point 30% overlapped sections, each of which is tapered in the time domain by applying a time-bandwidth product 4 prolate spheroidal taper function. The time series was prewhitened by applying a 48-point autoregressive filter to a lowpass filtered version of the original time series. Well-defined peaks in the spectrum are seen at the tidal periods and their harmonics. The spectrum is shown within an envelope representing one standard error.

variability, although direct visual examination of the time series, which extend from August 1994 to the beginning of January 1995 do suggest that there is fortnightly

variability as well. There is also evidence of a secular shift in the locus of heating of the TAG mound during the six month measurement period (Schultz *et al.* 1996).

Spectral analysis of diffuse effluent velocity (rather than temperature) time series reveal that these variations are predominantly diurnal. The power in the diurnal peak is approximately fives times that of the semi-diurnal peak for effluent velocity. The different spectral forms for the effluent temperature and velocity may be diagnostic of the nature of the internal hydrology of TAG. This is the subject of current investigation. Mechanisms that may modulate the response of a hydrothermal system to tidally modified boundary conditions are proposed below.

(*c*) *Mechanisms for tidal influence on hydrothermal flow and measurement*

Ocean tides modulate the seafloor pressure field, changing the value of hydrostatic pressure within the hydrothermal system. The variation in height of the water column loads the seafloor, which has finite rigidity, and which deforms in response to this tidal loading. The solid Earth also responds to astronomical tidal forces and acts to deform the oceanic lithosphere from below thus changing the state of stress at the seafloor. Changes in the horizontal velocity of the water column have an effect on the thermal boundary conditions on the seafloor. There are measurement issues related to the Bernoulli effect due to lateral tidal motions on open crack-dominated hydrothermal flow. We shall consider each of these cases in turn.

(i) *Temporal variability in seafloor thermal boundary conditions*

In § 3 we considered the effect of in-flow of seawater and out-flow of effluent on a model of flow within a cracked permeable structure. In regions of out-flow we imposed a boundary condition of zero thermal gradient, and in regions of in-flow a condition of zero temperature.

Tidal motions of the water column will alter the seafloor thermal boundary conditions similarly, forcing approximate Dirichlet and Neumann conditions to hold, depending upon the horizontal motions. At periods of peak tidal exchange, the strong motion of the tides will act to transport heat advectively and efficiently away from the outer surface of the cracked permeable hydrothermal system. At such times we may reasonably impose an approximate zero temperature condition at the boundary between the sea and the structure. Given peak tidal velocities within Mid-Ocean Ridge hydrothermal systems of *ca.* $20\ \mathrm{cm\ s^{-1}}$, (Lukashin, personal communication; Rudnicki 1990), very efficient lateral advection of heat into the water column is to be expected.

At periods of slack tidal exchange, a thin thermal boundary layer of the sort proposed by Little *et al.* (1988) is expected. In such a layer, vertical gradients in temperature are minimized.

The major effect of alternating between the peak-tidal-exhange and slack-tidal-exchange thermal boundary conditions is to perturb the temperature field inside the permeable medium, but only very close to its outer surface. There is little effect on the pattern of flow within the structure. While seemingly of little consequence, it is at the seawater–structure interface that conductive and advective heat flow measurements are made. The tidal variation in thermal boundary conditions may therefore have some effect on measurements made within the thickness of the thermal boundary layer.

(ii) *Bernoulli effects*

The lateral motion of the water column past an open channel either penetrating the interior of the permeable structure (e.g. a vent chimney), or any measurement system situated directly above the structure, would experience a vertical pressure gradient imposed by the lateral motion of fluids past the top of the chamber.

Bernoulli's equation relates the variation of pressure along a given streamline to the variation in speed of flow,

$$\tfrac{1}{2}\rho|\bar{u}|^2 + p = C_{\mathrm{S}}, \tag{5.1}$$

where $\bar{u}$ is the velocity of the flow, ρ is the density of the fluid, $\frac{1}{2}\rho|\bar{u}|^2$ is the kinetic energy per unit volume of the fluid, p is the pressure, and C_{S} is a constant along a given streamline S. One sees immediately that at points along a given streamline where velocity is high, pressure is low.

The practical consequence of Bernoulli's equation is that lateral flow of seawater around an obstacle such as a hydrothermal vent structure will tend to generate a pressure drop immediately above the opening of a vent or instrument orifice. This is the basic principle behind both the venturi tube and the pitot tube, devices which make use of the Bernoulli effect to measure the velocity of moving fluids.

It is conceivable that Bernoulli effects may have an impact on the velocity field immediately within and above vent orifices and sulphide structures, or in some configurations within instruments deployed to measure the temperature or velocity of effluent in situ. These effects may be larger in the presence of slip, i.e. when there are strong vertical gradients in the lateral flow of seawater past a structure. The presence of a viscous boundary layer on the outer surface of the hydrothermal mound or vent may provide such an environment. This might have an impact on time series measurements of the temperature of black smoker fluids made by inserting sensors directly into the vent orifice.

(iii) *Response of the seafloor to ocean tides and solid Earth deformations*

Seafloor hydrostatic pressure is modulated directly by ocean tides. Peak tidal amplitudes in the open ocean (generally semi-diurnal peaks are predominant) are no more than *ca.* 1 m (Schwiderski 1980). This presents a hydrostatic pressure variation of roughly one part in $2.5\text{–}4.0 \times 10^3$ at the surface of a typical seafloor hydrothermal system. The direct effect of this on the governing equations of flow, e.g. (3.1), (3.2) and (3.3), is small and depends on the confined or lithostatic pressure of the system, although a time-dependent element is introduced, and some small-scale effects may arise. This may be contrasted with the effects of changes in barometric pressure on continental aquifers and wells. Total barometric pressure on the Earth's surface may change by approximately five parts in 1×10^2 during the transition from low-to-high pressure fronts, an effect one-to-two orders of magnitude greater than that experienced by seafloor hydrothermal systems by tidal variations in hydrostatic pressure.

In continental systems changes in barometric pressure may depress or elevate the level of water in open artesian wells according to the relation (Bredehoeft 1967)

$$\frac{\mathrm{d}p_{\mathrm{b}}}{\mathrm{d}p} = -B, \tag{5.2}$$

where p_{b} is the barometric pressure. The constant of proportionality B, the 'barometric efficiency' a function of the porosity of the system, is seen to vary over the full

range of 0 to 1 in continental wells. Thus water levels in continental artesian wells may be influenced strongly by changes in barometric pressure. While this is not expected to be the case in seafloor systems, it is imprudent to dismiss completely the possible influence of time variations in hydrostatic pressure on the level of submarine aquifers.

The tidal dilation of continental aquifers also acts to displace the water level within the aquifer. Bredeheoft (1967) calculate the changes in aquifer water level associated with tidal potentials and find these range between 10^{-3} and 10^{-2} m. This is quite similar to water level fluctuations reported as due to Earth tides in slightly fractured crystalline rock (*ca.* 10^{-2} m) and in sediments (*ca.* 10^{-3} m) in the southeastern United States (Marine 1975). It is reasonable to expect a similar process to operate within submarine aquifers. The change in water levels in such a submarine system, if sufficiently large, might influence the advective flow of heat to the surface which might manifest itself as a signal with tidal periodicities. Further analysis is required before the plausibility of this mechanism can be evaluated properly.

Davis & Becker (1994) report on an anticorrelation between temperature and pressure within ODP Hole 858G, a drill hole penetrating deep into a sedimented hydrothermal system on the Juan de Fuca Ridge. Fang *et al.* (1993) also note a similar effect within pore pressure measured within marine sediments, and D. Orange (personal communication, 1996) has observed related effects on the sedimented seafloor of Monterey Canyon in California. Wang & Davis (1996) note that a pressure variation at the seafloor induces both an essentially instantaneous change in pressures at all depths within the seafloor (i.e. an elastic response) as well as an additional component of the pressure signal that diffuses downward with a depth-dependent attenuation (see also Crawford *et al.* 1991). The phase shift and amplitude attenuation of the tidally induced pressure change is frequency dependent and a function primarily of hydraulic diffusivity. The skin depth of the diffusion of the seafloor pressure disturbance is proportional to the reciprocal square-root of the product of diffusivity and period. For typical marine sediments, this is only a few metres. Wang & Davis (1996) suggest that internal contrasts in elastic properties (e.g. the presence of free gas) can give rise to large instantaneous pressure changes across layer boundaries, thus amplifying the otherwise small effect.

(iv) *Seafloor tidal deformation and modulation of permeability structure*

We consider a final consequence of the loading of the seafloor by ocean tides and the deformation of the solid Earth. Under the appropriate conditions it may be plausible to consider the sensitivity of the bulk permeability structure of the lithospheric hydrothermal system to seafloor deformations.

The compliance of the seafloor is the complex frequency domain function (i.e. transfer function) relating the deformation of the seafloor to the vertical normal stress due to the pressure imposed upon the seafloor by the water column. The vertical component of compliance may be written (Crawford *et al.* 1991)

$$\zeta(\omega) = \frac{u_z}{\tau_{zz}} = u_z \Big/ \left[\lambda\left(\frac{\partial u_x}{\partial x} + \frac{\partial u_z}{\partial z}\right) + 2\mu\frac{\partial u_z}{\partial z}\right], \tag{5.3}$$

where u_j is the particle displacement in the x_j direction, μ is the rigidity or shear modulus (the first Lamé parameter), λ is the second Lamé parameter, ρ is the density of the material, and τ_{zz} is the vertical stress imposed on the seafloor by the water column. The magnitude of vertical displacement of the seafloor is therefore related

to the imposed stress and the material properties of the seafloor (i.e. the Lamé parameters).

The unknown and potentially considerable degree of spatial heterogeneity of the elastic properties of an active hydrothermal system make it difficult to apply these concepts for modelling finer-scale tidally induced deformations. In such a case the approach of Crawford *et al.* (1991) in measuring simultaneously the seafloor pressure and displacement fields, and then inverting estimates of the vertical compliance for these material properties is quite promising. This provides a means to recover, usually in concert with allied seismic observations, the elastic properties of the lithosphere.

On the global scale, one may refer to globally averaged models of the Earth's elastic parameters. We have explored such an approach by making use of a series of computer programs distributed by H. G. Wenzel of the University of Karlsruhe. These codes use the PREM radially symmetric seismic model of elastic parameters of the Earth's crust and mantle, and by referring to Dehant (1987), Wahr (1981) and Zschau & Wang (1987), make it possible to relate the tidal potential functions to solid Earth deformations. The Earth-tide induced deformations of the Earth's surface are given (Bredehoeft 1967)

$$u_r = \bar{h}\frac{W_2}{g}, \qquad u_\theta = \frac{\bar{l}}{g}\frac{\partial W_2}{\partial \theta}, \qquad u_\phi = \frac{\bar{l}}{g}\sin\theta\frac{\partial W_2}{\partial \phi}, \tag{5.4}$$

where $\bar{h}$ and $\bar{l}$ are 'Love numbers' (taken to be constant at the Earth's surface) which relate the true displacements to those predicted by equilibrium tide theory, g is gravitational acceleration, W_2 is the lunar/solar disturbing potential, r is the radial direction, θ is the colatitude, and ϕ is the longitude, positive eastward. The Love numbers may be determined from the elastic properties and the density of the material in question (Takeuchi 1950).

The solid Earth tidal displacements of the Earth's surface relative to the geoid may be calculated using the approach above. Displacements of nearly 1 m peak are calculated. Of course, this value is based on an underlying radially symmetric elastic model which may not reflect accurately the local structure within the lithospheric hydrothermal system.

Tsuruoka *et al.* (1995) have used a similar approach to study the correlation between tides and triggering of earthquakes. This work includes the contributions to the seafloor stress field of both solid Earth tides and ocean tidal loading forces and thus is particularly appropriate for the present discussion. The maximum incremental tidal shear stress reported by Tsuruoka *et al.* is *ca.* 4000 Pa, peak-to-peak with a predominantly semi-diurnal periodicity.

In an isotropic medium it is possible to relate the normal stresses to the normal strains through the material constants λ and μ (Bredehoeft 1967)

$$\sigma_{rr} = \lambda\Delta + 2\mu\epsilon_{rr}, \qquad \sigma_{\theta\theta} = \lambda\Delta + 2\mu\epsilon_{\theta\theta}, \qquad \sigma_{\phi\phi} = \lambda\Delta + 2\mu\epsilon_{\phi\phi}, \tag{5.5}$$

where the dilatation $\Delta = \epsilon_{rr} + \epsilon_{\theta\theta} + \epsilon_{\phi\phi}$.

By substituting the radial normal component of strain the dilatation is written

$$\Delta = \frac{1-2\nu}{1-\nu}(\epsilon_{\theta\theta} + \epsilon_{\phi\phi}), \tag{5.6}$$

where ν is Poisson's ratio. In a spherical radially symmetric Earth the horizontal components of the strain may be solved for by calculating the displacements and

their horizontal derivatives,

$$\epsilon_{\theta\theta} = \frac{1}{r}\left(\frac{\partial u_\theta}{\partial \theta} + u_r\right), \qquad \epsilon_{\phi\phi} = \frac{1}{r}\left(\frac{1}{\sin\theta}\frac{\partial u_\phi}{\partial \phi} + u_\theta \frac{\cos\theta}{\sin\theta} + u_r\right). \tag{5.7}$$

Presuming that compressional stresses due to tidal effects are of similar order to the shear stresses calculated by Tsuruoka *et al.* (1995), i.e. *ca.* 4000 Pa peak-to-peak, and taking $\nu \approx \frac{1}{4}$ we find that $\Delta \sim 10^{-8}$, a figure in general agreement with that calculated for the lunar semi-diurnal component by Bredeheoft (1967), and by Wenzel's computer code.

(v) *A model of lithospheric permeability*

While Δ is only a small volumetric change, the effects of this change on the effective permeability of a cracked permeable system may be significant. We examine this by representing the permeability of an idealized medium as that due to a network of fine interconnected capillary tubes. Within such a tube, 'Hagen–Poiseuille' or pipe flow will hold where

$$u(r_\mathrm{p}) = -\frac{\partial p}{\partial x}\frac{(a_\mathrm{p}^2 - r_\mathrm{p}^2)}{4\mu}, \tag{5.8}$$

where x is the direction of the axis of the pipe, a_p is the radius of the pipe, r_p is the radial distance from the centre of the pipe, μ is the viscosity of the fluid, and $u(r_\mathrm{p})$ is the velocity of the fluid in the x direction. The Reynolds number is defined $Re = \rho\hat{u}2a_\mathrm{p}/\mu$, where $\hat{u}$ is the average velocity in the pipe, given below. For a given pressure, the average velocity of fluid flowing through the capillary tube is proportional to the square of the tube's radius.

The mass flux of fluid passing through the pipe is given by,

$$\int_0^{a_\mathrm{p}} \rho 2\pi r_\mathrm{p} u(r_\mathrm{p})\,\mathrm{d}r_\mathrm{p} = -\frac{\pi\rho}{8\mu}\frac{\partial p}{\partial x}a_\mathrm{p}^4, \tag{5.9}$$

thus the mass flux is proportional to the fourth power of the pipe radius and the average velocity $\hat{u}$ is the mass flux divided by $\pi\rho a_\mathrm{p}^2$.

Hagen–Poiseuille flow holds for pipe geometries of small Reynolds number. For a given set of conditions there exists a critical pipe radius (i.e. Reynolds number) where the flow begins to transition from laminar to turbulent. In turbulent flow the flow rate through the pipe will be less for a given pressure gradient than for laminar flow (Tritton 1988).

The permeability of a medium consisting of n parallel-aligned pipes of equal radius aligned at an angle θ to the pressure gradient, embedded within an impermeable matrix is (Phillips 1991)

$$\boldsymbol{k} = \frac{\phi a_\mathrm{p}^2}{32}\boldsymbol{A}, \tag{5.10}$$

where the porosity $\phi = n\pi a_\mathrm{p}^2$, and where $\boldsymbol{A}$ is a 3×3 matrix of sines and cosines. For capillary tubes orientated randomly relative to the pressure gradient,

$$k = \frac{\phi a_\mathrm{p}^2}{96}. \tag{5.11}$$

This discussion does not depend critically on the assumption that permeability is regulated entirely by systems of capillary tubes (obviously a gross simplification).

Phillips (1991) notes that if tubes are replaced by an isotropic system of plane fractures of crack width δ_w, the permeability is

$$k = \frac{\phi \delta_w^2}{36}. \tag{5.12}$$

Section 3 makes it clear that providing a sufficient supply of effluent to the surface of a hydrothermal system requires that the permeable system must have cracks embedded within it. Throughout much of the volume of the structure flow will obey D'arcy's Law, but purely D'arcy flow cannot explain the large velocities and fluxes observed in typical diffuse flow fields. Therefore in such systems bulk transport of fluids is accelerated by the presence of cracks.

The permeability of typical oceanic basalts is constrained poorly, but values in the range 10^{-19}–10^{-13} m^{-2} have been measured, e.g. in DSDP Hole 504B, Costa Rica Rift (Williams *et al.* 1986).

If the bulk permeability is crack-dominated, then to achieve the small observed permeabilities of oceanic basalt implies that the crack widths δ_w of (5.12), or pipe radii a_p of (5.11) are on average likely to be exceedingly small. The dilatation Δ is likely to be taken up largely through constriction of these small voids, thus the commensurate change in the size of the cracks is likely to be large. This is an area of current research, and we are investigating coupling boundary element solutions for the deformation of cracks and tubes to models of lithospheric strain due to ocean tidal loading and solid Earth deformations.

In the event that the $O(10^{-8})$ typical dilatation does lead to significant changes in mean pipe radius, particularly if the mean pipe flow path is represented by convoluted and tortuous pipes and cracks, the small dilatation may result in nearly unbounded changes in bulk permeability. If the constriction forces the Reynolds number beyond the critical range, flow will transition from laminar to turbulent, amplifying these effects further. Such modulations of effective permeability will lead to changes in the flow velocity field with tidal periodicities.

It has already been noted that the mass flux scales with the fourth power of pipe radius. The advective heat flux through a pipe will therefore also scale with the fourth power, which would then couple into the permeable part of the system, in a complex way, through (3.2). It may be expected qualitatively that tidal effects on the temperature of the fluids exiting the hydrothermal system may be more pronounced that those seen in the velocity of those fluids.

The differences between the spectral characteristics of the temperature and the velocity measurements of diffuse flow on the TAG hydrothermal mound have been pointed out previously. The frequency-dependence of seafloor compliance may provide a means of modulating the spectrum of the effluent temperature and velocity in different ways. The stresses imposed on the lithosphere by diurnal ocean tides will tend to penetrate to greater depths than those due to semi-diurnal tides. This too is an area of current research.

(vi) *Continental analogues*

Rinehart (1980) discusses the relationship between continental solid Earth tidal deformations and the average interval between geyser eruptions in geothermal systems. In addition to the familiar diurnal and semi-diurnal modulations, he considers further the fortnightly, semi-annual and even longer period astronomical tidal cycles and corresponding deformations. Rinehart concurs that the elastic effect on com-

petent rocks results in dilatations of order 10^{-7}–10^{-8}. He interprets the inelastic deformation to arise from the compression and dilatation of the pores and voids within such geothermal systems, and that this may be governing the tidal response.

In continental systems, the diurnal and semi-diurnal tides have little appreciable effect on geyser activity, despite these being associated with the largest elastic dilatation of any of the solid Earth tides. There is, however, a striking correlation between the fortnightly tidal peak, as well as even longer period tidal variations extending to months and years, and the mean interval between geyser eruptions at the Riverside, Old Faithful, Grand and Steamboat geysers in North America (Rinehart 1980).

The possibility that very long period, or secular variations in the permeability structure of the oceanic lithosphere may be linked to tidal loading and deformation may lead to very considerable uncertainty in efforts to quantify hydrothermal fluxes made from repeated spot measurement episodes over sequential field seasons. Rather, combining hydrothermal measurements with geodetic observations, and doing so in the form of quasi-permanent seafloor observatories may prove the most effective means of studying the interaction between the oceanic lithosphere and the hydrosphere.

This paper was prepared under the partial support of grants received from the Natural Environment Research Council/BRIDGE Programme, and the European Union MAST III Programme. The authors thank P. Dickson for her calculations of flow within a cracked permeable medium, and R. James and M. Greaves for their chemical analysis of the Medusa fluid samples. We acknowledge the dedication of our workshop staff in designing and building the instruments used to obtain the samples (particularly M. Walker, S. Riches, and P. Smith), and also the crews of the RV Keldysh and Atlantis II, and submersibles MIR1, MIR2 and Alvin. A.S. is indebted to the late Clive Lister, to whom this paper is dedicated, for many valuable conversations over the years, for assistance in construction of critical parts of his earlier instruments, and for being a voice of reason. Contribution number 4828, Department of Earth Sciences and Institute of Theoretical Geophysics, University of Cambridge.

References

Alt, J. C., Lonsdale, P., Haymon, R. & Muehlenbachs, K. 1987 Hydrothermal sulfide and oxide deposits on seamounts near 21° N East Pacific Rise. *Geol. Soc. Am. Bull.* **98**, 157–168.

Baker, P. A., Stout, P. M., Kastner, M. & Elderfield, H. 1991 Large-scale lateral advection of seawater through oceanic crust in the central equatorial Pacific. *Earth Planet. Sci. Lett.* **105**, 522–533.

Baker, E. T., Massoth, G. J., Walker, S. L. & Embley, R. W. 1993 A method for quantitatively estimating diffuse and discrete hydrothermal discharge. *Earth Planet. Sci. Lett.* **118**, 235–249.

Baker, E. T., German, C. R. & Elderfield, H. 1995 Hydrothermal plumes over spreading-center axes: global distributions and geological inferences. In *Seafloor hydrothermal systems* (ed. S. E. Humphris, R. A. Zierenberg, L. S. Mullineaux & R. E. Thomson), pp. 47–71. (Geophysical Monograph 91.) Washington, DC: AGU.

Becker, K. & Von Herzen, R. P. 1996 Pre-drilling observations of conductive heat flow at the TAG active mound using Alvin. *Proc. ODP Initial Rep.* **158**, 23–29.

Bischoff, J. L. & Rosenbauer, R. J. 1985 An empirical equation of state for hydrothermal seawater (3.2 percent NaCl). *Am. Jl Sci.* **285**, 725–763.

Bischoff, J. L. & Rosenbauer, R. J. 1989 Salinity variations in submarine hydrothermal systems by layered double-diffusive convection. *J. Geol.* **97**, 613–623.

Bredehoeft, J. D. 1967 Response of well-aquifer systems to Earth tides. *J. Geophys. Res.* **72**, 3075–3087.

Butterfield, D. A. & Massoth, G. J. 1994 Geochemistry of North Cleft Segment vent fluids – temporal changes in chlorinity and their possible relation to recent volcanism. *J. Geophys. Res.* B **99**, 4951–4968.

Butterfield, D. A., McDuff, R. E., Mottl, M. J., Lilley, M. D., Lupton, J. E. & Massoth, G. J. 1994 Gradients in the composition of hydrothermal fluids from the Endeavour Segment vent field – phase-separation and brine loss. *J. Geophys. Res.* B **99**, 9561–9583.

Carlson, R. L. & Johnson, H. P. 1994 On modeling the thermal evolution of the oceanic upper mantle: an assessment of the cooling plate model. *J. Geophys. Res.* B **99**, 3201–3214.

Chen, C.-T. A. & Marshall, W. L. 1982 Amorphous silica solubilities. IV. Behavior in pure water and aqueous sodium chloride, sodium sulfate, magnesium chloride, and magnesium sulfate solutions up to 350 °C. *Geochim. Cosmochim. Acta* **46**, 279–287.

Corliss, J. B., Dymond, J., Gordon, L. I., Edmond, J. M., Von Herzen, R. P., Ballard, R. D., Green, K., Williams, D., Bainsbridge, A., Crane, K. & Van Andel, T. H. 1977 Submarine thermal springs on the Galapagos Rift. *Science* **203**, 1073–1083.

Crawford, W. C., Webb, S. C. & Hildebrand, J. A. 1991 Seafloor compliance observed by long-period pressure and displacement measurements. *J. Geophys. Res.* B **96**, 16 151–16 160.

Davis, E. E. & Lister, C. R. B. 1974 Fundamentals of ridge crest topography. *Earth Planet. Sci. Lett.* **21**, 405–413.

Davis, E. E. *et al.* 1992 Flank flux: an experiment to study the nature of hydrothermal circulation in young oceanic crust. *Can. Jl Earth Sci.* **29**, 925–952.

Dehant, V. 1987 Tidal parameters for an inelastic Earth. *Phys. Earth Planet. Int.* **49**, 97–116.

Delaney, J. R., Mogk, D. W. & Mottl, M. J. 1987 Quartz-cemented breccias from the Mid-Atlantic Ridge: sampled of a high-salinity hydrothermal upflow zone. *J. Geophys. Res.* B **92**, 9175–9192.

Dickson, P., Schultz, A. & Woods, A. 1995 Preliminary modelling of hydrothermal circulation within mid-ocean ridge sulphide structures. In *Hydrothermal vents and processes* (ed. L. M. Parson, C. L. Walker & D. R. Dixon), pp. 145–158. Geological Society Special Publication no. 87.

Edmond, J. M., Campbell, A. C., Palmer, M. R., Klinkhammer, G. P., German, C. R., Edmonds, H. N., Elderfield, H., Thompson, G. & Rona, P. 1995 Time series studies of vent fluids from the TAG and MARK sites (1986, 1990) Mid-Atlantic Ridge: a new solution chemistry model and a mechanism for Cu/Zn zonation in massive sulphide orebodies. In *Hydrothermal vents and processes* (ed. L. M. Parson, C. L. Walker & D. R. Dixon), pp. 77–86. Geological Society Special Publication no. 87.

Edmonds, H. N. & Edmond, J. N. 1995 A three-component mixing model for ridge-crest hydrothermal fluids. *Earth Planet. Sci. Lett.* **134**, 53–67.

Elder, J. W. 1965 Physical processes in geothermal areas. In *Terrestrial heat flow* (ed. W. H. K. Lee), pp. 211–239. (Geophysical Monograph 8.) Washington, DC: AGU.

Elderfield, H. & Schultz, A. 1996 Mid-ocean ridge hydrothermal fluxes and the chemical composition of the ocean. *A. Rev. Earth Planet. Sci.* **24**, 191–224.

Fang, W. W., Langseth, M. G. & Schultheiss, P. J. 1993 Analysis and application of *in situ* pore pressure measurements in marine sediments. *J. Geophys. Res.* **98**, 7921–7938.

Fehn, U., Green, K. E., Von Herzen, R. P. & Cathles, L. M. 1983 Numerical models for the hydrothermal field at the Galapagos spreading center. *J. Geophys. Res.* B **88**, 1033–1048.

Franklin, J. M., Sangster, D. M. & Lydon, J. W. 1981 Volcanic-associated massive sulphide-deposits (ed. B. J. Skinner). *Econ. Geol.* **75**, pp. 485–627.

Gallahan, W. E. & Duncan, R. A. 1994 Spatial and temporal variability in crystallization of celadonites within the Troodos ophiolite, Cyprus: implications for low-temperature alteration of the oceanic crust. *J. Geophys. Res.* B **99**, 3147–3161.

Hartline, B. K. & Lister, C. R. B. 1981 Topographic forcing of supercritical convection in a porous medium such as the oceanic crust. *Earth Planet. Sci. Lett.* **55**, 75–86.

Hendershott, M. C. 1981 Long waves and ocean tides. In *Evolution of physical oceanography* (ed. B. A. Warren & C. Wunsch), pp. 292–341. Cambridge, MA: MIT Press.

Honnorez, J. 1981 The aging of the oceanic crust at low-temperatures. In *The sea*, vol. 7: *The oceanic lithosphere* (ed. E. Emiliani), pp. 525–588. New York: Wiley.

Humphris, S. E., Herzig, P. M., Miller, D. J. & ODP leg 158 Shipboard Scientific Party 1995 The internal structure of an active sea-floor massive sulphide deposit. *Nature* **377**, 713–716.

James, R. H. 1995 Chemical processes in submarine hydrothermal systems at the Mid-Atlantic Ridge. Ph.D. thesis, University of Cambridge.

James, R. H. & Elderfield, H. 1996 Chemistry of ore-forming fluids and mineral formation rates in an active hydrothermal sulphide deposit on the Mid-Atlantic Ridge. *Geology* **24**, 1147–1150.

Johnson, H. P., Becker, K. & Von Herzen, R. 1993 Near-axis heat flow measurements on the Northern Juan de Fuca Ridge: implications for fluid circulation in oceanic crust. *Geophys. Res. Lett.* **20**, 1875–1878.

Kadko, D., Baker, E., Alt, J. & Baross, J. 1994 Global impact of submarine hydrothermal processes. Report of the RIDGE/VENTS Workshop, US Ridge Inter-Disciplinary Global Experiments, Boulder, Colorado.

Kennedy, G. C. 1950 A portion of the system silica-water. *Econ. Geol.* **45**, 629–653.

Lalou, C., Thompson, G., Arnold, M., Brichet, E., Druffel, E. & Rona, P. 1990 Geochronology of TAG and Snakepit hydrothermal fields, Mid Atlantic Ridge: witness to a long and complex hydrothermal history. *Earth Planet. Sci. Lett.* **97**, 113–128.

Le Pichon, X. & Langseth Jr, M. G. 1969 Heat flow from mid-ocean ridges and sea-floor spreading. *Tectonophys.* **8**, 319–344.

Lister, C. R. B. 1972 On the thermal balance of a mid-ocean ridge. *Geophys. Jl R. Astr. Soc.* **26**, 515–535.

Little, S. A., Stolzenbach, K. D. & Grassle, F. J. 1988 Tidal current effects on temperature in diffuse hydrothermal flow: Guaymas Basin. *Geophys. Res. Lett.* **15**, 1491–1494.

Marine, I. W. 1975 Water level fluctuations due to Earth tides in a well pumping from a slightly fractured crystalline rock. *Water Resources Res.* **11**, 165–173.

McKenzie, D. P. 1967 Some remarks on heat flow and gravity anomalies. *J. Geophys. Res.* **72**, 6261–6273.

Melchior, P. 1956 Sur l'effet des marées terrestes dans les variations de nivaeu observée dan les puits, en particular au sondage de Turnhout (Belgium). *Commun. Obs. R. Belgique* **108**, 7–28.

Mills, R. A., Thomson, J., Elderfield, H. & Rona, P. A. 1993 Pore water chemistry of metalliferous sediments from the Mid-Atlantic Ridge: diagenesis and low-temperature fluxes. *Eos* **74**, 10.

Morton, J. L. 1984 Oceanic spreading centers: axial magma chambers, thermal structure, and small scale ridge jumps. Ph.D. thesis, Stanford University, California.

Morton, J. L. & Sleep, N. H. 1985 A mid-ocean ridge thermal model: constraints on the volume of axial hydrothermal heat flux. *J. Geophys. Res.* B **90**(13), 11 345–11 353.

Morton, J. L., Sleep, N. H., Normark, W. R. & Tompkins, D. H. 1987 Structure of the Southern Juan de Fuca Ridge from seismic reflection records. *J. Geophys. Res.* B **92**, 11 315–11 326.

Monfort, M. & Schultz, A. 1988 Timeseries measurements of hydrothermal vent temperature and diffuse percolation velocity: results from an ALVIN submersible program, Endeavour Segment, Juan de Fuca Ridge. *Eos* **69**, 1484.

Parsons, B. & Sclater, J. G. 1977 An analysis of the variation of ocean floor bathymetry and heat flow with age. *J. Geophys. Res.* **82**, 803–827.

Phillips, O. M. 1991 *Flow and reactions in permeable rocks.* New York: Cambridge University Press.

Phipps Morgan, J. & Chen, Y. J. 1993 The genesis of oceanic crust: magma injection, hydrothermal circulation, and crustal flow. *J. Geophys. Res.* B **98**, 6283–6297.

Rinehart, J. S. 1980 *Geysers and geothermal energy.* New York: Springer.

Rona, P. A. & Trivett, D. A. 1992 Discrete and diffuse heat transfer at ASHES vent field, Axial Volcano, Juan de Fuca Ridge. *Earth Planet. Sci. Lett.* **109**, 57–71.

Rona, P., Hannington, M. D., Raman, C. V., Thompson, G., Tivey, M. K., Humphris, S. E., Lalou, C. & Peterson, S. 1990 Active and relict sea-floor hydrothermal mineralization at the TAG hydrothermal field. *Econ. Geol.* **88**, 1989–2017.

Rosenberg, N. D., Lupton, J. E., Kadko, D., Collier, R., Lilley, M. D. & Pak, H. 1988 Estimation of heat and chemical fluxes from a seafloor hydrothermal vent field using radon measurements. *Nature* **334**, 604–607.

Rudnicki, M. D. 1990 Hydrothermal plumes at the Mid-Atlantic Ridge. Ph.D. thesis, University of Cambridge.

Rudnicki, M. D. & Elderfield, H. 1992 Theory applied to the Mid-Atlantic Ridge hydrothermal plumes: the finite difference approach. *J. Volcanology Geotherm. Res.* **50**, 163–174.

Schultz, A., Delaney, J. R. & McDuff, R. E. 1992 On the partitioning of heat flux between diffuse and point source seafloor venting. *J. Geophys. Res.* **97**, 12 299–12 314.

Schultz, A., Dickson, P. & Elderfield, H. 1996 Temporal variations in diffuse hydrothermal flow at TAG. *Geophys. Res. Lett.* **23**, 3471–3474.

Schwiderski, E. W. 1980 On charting global ocean tides. *Rev. Geophys. Space Phys.* **18**, 243–268.

Sclater, J. G., Jaupart, C. & Galson, D. 1980 The heat flow through oceanic and continental crust and the heat loss of the Earth. *Rev. Geophys. Space Phys.* **18**, 2269–2311.

Sleep, N. H. 1975 Formation of oceanic crust: some thermal constraints. *J. Geophys. Res.* **80**, 4037–4042.

Stein, C. A. & Stein, S. 1992 A model for the global variation in oceanic depth and heat flow with lithospheric age. *Nature* **359**, 123–129.

Stein, C. A. & Stein, S. 1994 Constraints on hydrothermal heat flux through the oceanic lithosphere from global heat flow. *J. Geophys. Res.* B **99**, 3081–3095.

Stein, C. A., Stein, S. & Pelayo, A. M. 1995 Heat flow and hydrothermal circulation. In *Seafloor hydrothermal systems* (ed. S. E. Humphris, R. A. Zierenberg, L. S. Mullineaux & R. E. Thomson), pp. 425–445. (Geophysical Monograph 91.) Washington, DC: AGU.

Takeuchi, H. 1950 On the Earth tide of the compressible Earth of variable density and elasticity. *Eos* **31**, 651–689.

Thomson, D. J. 1982 Spectrum estimation and harmonic analysis. *Proc. IEEE* **70**, 1055–1096.

Tivey, M. K., Humphris, S. E., Thompson, G., Hannington, M. D. & Rona, P. A. 1995 Deducing patterns of fluid-flow and mixing within the TAG active hydrothermal mound using mineralogical and geochemical data. *J. Geophys. Res.* B **100**, 12 527–12 555.

Tritton, D. J. 1988 *Physical fluid dynamics*, 2nd edn. Oxford: Oxford Science Publications, Clarendon Press.

Tsuruoka, H., Ohtake, M. & Sato, H. 1995 Statistical test of the tidal triggering of earthquakes: contribution of the ocean tide loading effect. *Geophys. Jl Int.* **122**, 183–194.

Turner, J. S. & Gustafson, L. B. 1978 The flow of hot saline solutions from vents in the sea floor – some implications for exhalative massive sulfide and other ore deposits. *Econ. Geol.* **73**, 1082–1100.

Turner, J. S. & Campbell, I. H. 1987 A laboratory and theoretical study of the growth of 'black smoker' chimneys. *Earth Planet. Sci. Lett.* **82**, 36–48.

Vera, E. E. & Diebold, J. B. 1994 Seismic imaging of oceanic layer 2A between 9°30′ and 10° N on the East Pacific Rise from two-ship wide-aperature profiles. *J. Geophys. Res.* B **99**, 3031–3041.

Von Damm, K. L., Edmond, J. M., Grant, B., Measures, C. I., Walden, B. & Weiss, R. F. 1985 Chemistry of submarine hydrothermal solutions at 21° N, East Pacific Rise. *Geochim. Cosmochim. Acta* **49**, 2197–2220.

Wahr, J. M. 1981 Body tides on an elliptical, rotating, elastic and oceanless Earth. *Geophys. Jl R. Astr. Soc.* **64**, 677–703.

Wang, K. & Davis, E. E. 1996 Theory for the propagation of tidally induced pore pressure variations in layered subseafloor formations. *J. Geophys. Res.* B **101**, 11483–11495.

Wheat, C. G. & Mottl, M. J. 1994 Hydrothermal circulation, Juan de Fuca Ridge eastern flank: factors controlling basement water composition. *J. Geophys. Res.* B **99**, 3067–3080.

Williams, C. F., Narasimhan, T. N., Anderson, R. N., Zoback, M. D. & Becker, K. 1986 Convection in the oceanic crust: simulation of observations from Deep Sea Drilling Project Hole 504B, Costa Rica Rift. *J. Geophys. Res.* B **91**, 4877–4889.

Zschau, J. & Wang, R. 1987 Imperfect elasticity in the Earth's mantle: implications for Earth tides and long period deformations. In *Proc. 9th. Int. Symp. on Earth Tides* (ed. J. T. Kuo), pp. 605–629. Stuttgart: Schweizerbartsche Verlagsbuchhandlung.